Subgraphs and Motifs in a Dynamic Airline Network

Marius Agasse-Duval, Steve Lawford

Subgraphs and Motifs in a Dynamic Airline Network*

Marius Agasse-Duval and Steve Lawford

ENAC, University of Toulouse

Abstract

How does the small-scale topological structure of an airline network behave as the network evolves? To address this question, we study the dynamic and spatial properties of small undirected subgraphs using 15 years of data on Southwest Airlines' domestic route service. We find that this real-world network has much in common with random graphs, and describe a possible power-law scaling between subgraph counts and the number of edges in the network, that appears to be quite robust to changes in network density and size. We use analytic formulae to identify statistically over- and under-represented subgraphs, known as motifs and anti-motifs, and discover the existence of substantial topology transitions. We propose a simple subgraph-based node ranking measure, that is not always highly correlated with standard node centrality, and can identify important nodes relative to specific topologies; and investigate the spatial "distribution" of the triangle subgraph using graphical tools. Our results have implications for the way in which subgraphs can be used to analyze real-world networks.

*We are grateful to Karim Abadir, Gergana Bounova, Pascal Lezaud, Chantal Roucolle and Miguel Urdanoz for helpful comments and suggestions. We also thank Patrick Senac for supporting this project: Agasse-Duval was partially funded by an ENAC summer research grant. Correspondence can be addressed to Steve Lawford, ENAC (DEVI), 7 avenue Edouard Belin, CS 54005, 31055, Toulouse, Cedex 4, France; email: steve.lawford@enac.fr. The visualization, subgraph analysis, and motif detection tools used in this paper were coded by the authors in Python 2.7. The usual caveat applies. PACS numbers: 02.10.Ox (Combinatorics; graph theory), 89.40.Dd (Air transportation), 89.65.Gh (Economics; econophysics; financial markets; business and management), 89.75.-k (Complex systems). Keywords: Airline network, Graph theory, Network motif, Scaling, Subgraph.

1 Introduction

A network *motif* is a connected subgraph, usually with a small number of nodes, that occurs significantly more often in a real-world network than it does in an ensemble of appropriately-chosen random graphs. Motifs were first introduced by Milo et al. [51], who applied them to biochemical gene regulation networks, ecosystem food webs, neuronal connectivity networks, sequential logic electronic circuits, and a network of hyperlinks from the World Wide Web.[1] They found evidence that distinct sets of motifs are associated to different types of network, and suggest that motifs are basic structural elements, or topological interaction patterns, each of which may perform precise specialized functions, and that can be used to define universal network classes (e.g., evolutionary, information processing, etc.). Their paper was rapidly followed by many subsequent studies that looked for motifs in biological data, and in particular in gene regulation and neuroanatomical networks e.g. Alon [3], Dobrin et al. [21], Prill et al. [56], Sporns and Kötter [63], Yeger-Lotem et al. [77] and, more recently, Chen et al. [13] and Wu et al. [74]. However, the presence and interpretation of motifs in economic or transportation networks has received very little attention.

Graph-theoretic research on transportation networks typically focuses on macroscopic features such as network diameter, or microscopic measures that include unweighted node centrality to identify "important" nodes. In this paper, we count small, possibly overlapping, subgraphs and identify motifs in a transportation network, using 15 years of data on the U.S. domestic airport–airport route network of one of the world's largest passenger carriers: Southwest Airlines. We explore subgraph-based "mesoscopic" measures that fall between the local and global extremes, and ask the following questions: (a) do topological motifs arise in an airline network, and can their function or existence be interpreted in terms of the firm's strategy or business activity? (b) is there any variation and/or regularity in the number of subgraphs or motifs that are observed over time? (c) can subgraph-based centrality measures give different, yet informative, rankings to standard node centrality measures such as degree or betweenness? (d) by combining topological subgraphs with the spatial properties of an airline network (i.e., the nodes have a fixed geographical position), can we say anything interesting about the spatial "size" or "distribution" of such subgraphs over time?

The networks that we study in this paper have several notable features. First, they are very small, with no more than 88 nodes and 522 edges, in 2013Q4 (Section 2.1). By contrast, many real-world networks are extremely large. For example, Facebook and Twitter reported 2.01 billion and 328 million monthly active users, respectively, in the second quarter of 2017 (Facebook [28], Twitter [65]). The academic search engine Google Scholar covered an estimated 160 million indexed documents in 2014 (Orduña-Malea et al. [55]). The Stanford Large Network Dataset Collection (Leskovec and Krevl [47]) lists more than 90 large technological, social, communication and other graphs (or subgraphs) with thousands to millions of nodes and edges. The small size of our networks has significant implications for the algorithms and analysis that we are able to apply: in some cases, we use naïve algorithms with relatively poor asymptotic runtime performance, since these execute very fast on our data, and we do not need more sophisticated techniques. Second, airports and routes represent the topology of a human-made technological network, and their evolution will intimately reflect a carrier's strategic, economic and operational decisions, and constraints (e.g. regulatory, geographical). In that case, we might expect the interpretation of graph-based measures and motif occurrence to be very different to that for naturally-evolving biological networks, or for social networks on (say) collaborations between scientists or informal links between company executives.

We make the following specific contributions:

[1] An early study by some of these authors presented a specific application of motifs to genetics (Shen-Orr et al. [61]).

- We consider small (3- and 4-node) undirected subgraphs (Section 2). This choice enables us to use analytical formulae for enumeration in every case, and lets us avoid more difficult computational problems and algorithmic complexity. We list the set of nodes that make up each instance of each type of subgraph using a brute-force algorithm, but once again the small size of both the subgraphs and the real networks means that this procedure runs very rapidly on our data. An appropriate choice of loop indexes, based on node ordering and subgraph symmetry, allows us to count each subgraph instance once only (we use the analytical formulae as a check on the numerical procedures). We then characterize subgraphs as motifs (Section 2.4), by reference to two null random networks, chosen to have some of the same characteristics as the real network, namely the Erdős-Rényi random graph $G(n,p)$, and a rewiring model closely inspired by Milo et al. [51]. None of these individual aspects are entirely novel, but together they provide a practical method for analyzing subgraphs, and for finding small motifs in economic and transportation networks.

- We investigate dynamic variation in the number of subgraphs and motifs, by repeating the above steps for each quarterly network in the period 1999Q1 to 2013Q4 (Sections 2.2 – 2.4). We find that the number of subgraphs of a given type generally increases over time, as the size of the network grows. While this is not surprising, we also discover a possible power-law scaling regularity between subgraph count and number of edges m in the network, of the form $y = Am^{\beta}$. This scaling is stable across a wide range of number of edges and is quite robust to changes in network density. There is also evidence that the "slope coefficient" (power-law exponent) β is related to the number of nodes in some networks. Using a mathematical model we show that the apparent robustness may be an artifact. We draw comparisons with the implied scaling properties of an Erdős-Rényi random graph, and suggest that the airline network has some similar aggregate behaviour to a random graph.

- We describe several applications of subgraphs to the descriptive analysis of networks (Sections 2.5.1 and 2.5.2). First, we propose a simple new subgraph-based method to rank nodes, using the number of a particular type of subgraph in a network that contain a given node, and show that it can add new information beyond that which is captured by standard measures such as degree or betweenness centrality, for specific local topologies. We compare our results with the more general "subgraph-centrality" measure of node importance due to Estrada and Rodríguez-Velázquez [27], which we find to be highly correlated with degree (and other standard) centrality measures on our data. Second, we examine the dynamic spatial distribution of the triangle subgraph, based on standard geometric calculations of the size and center of the triangle, and show that it suggests a clear spatial shift in the concentration of network activity over time.

Our work is based on a large literature in graph theory and complex systems, and we discuss this related research in Section 3. All proofs, and some figures and notation, are collected in Appendices A – C.

2 Subgraphs and Motifs

We begin with an overview of the relevant tools of graph theory that we will use in this paper. Major monographs on the subject include mathematical aspects (Diestel [20]), applications to social networks and economics (Jackson [41]), and algorithms (Jungnickel [43]). Algorithms for graph search, shortest path length, and maximum flow, are also covered in detail by the excellent Cormen et al. [18, Section 6]. The

comprehensive survey by Newman [53] provides a complex systems perspective. A *graph* is an ordered pair $G = (V(G), E(G))$, where $V(G)$ is a set of *nodes* and $E(G)$ is a set of *edges* $E(G) \subseteq V(G) \times V(G)$. When there is no ambiguity, we write $V = V(G)$ and $E = E(G)$. The number of nodes and edges are denoted by $n = |V|$ and $m = |E|$ respectively. We generally refer to a graph by its unique $n \times n$ *adjacency matrix* g, which has representative element $(g)_{ij}$. In this paper, we consider *simple* (no self-links or multiple edges) undirected and unweighted graphs, so that $(g)_{ii} = 0$ (no self-links), $(g)_{ij} = (g)_{ji}$ (undirected) and $(g)_{ij} \in \{0,1\}$ (unweighted, no multiple edges). We use $(i,j) \in E$ to denote an edge between nodes i and j, and say that they are *directly-connected*. A *walk* between nodes i and j is a sequence of edges $\{(i_q, i_{q+1})\}_{q=1,\ldots,Q}$ such that $i_1 = i$ and $i_{Q+1} = j$. A *path* is a walk containing distinct nodes. A graph is *connected* if there is a path between any pair of nodes i and j. We assume that every theoretical network that we discuss will be connected and, furthermore, all of our empirical networks are also connected. A *cycle* (or a *simple cycle*) is a walk (or path) that starts and ends at the same node. The *diameter* (or *average path length*) is the maximum (or mean) shortest path length across all pairs of nodes in a graph. The *degree* $k_i = \sum_j (g)_{ij}$ is the number of nodes that are directly-connected to node i, and the *degree distribution* $P(k)$ is the probability distribution of k over G.[2] In a *k-regular* graph, every node has degree k. The *(1-degree) neighbourhood* of node i in G is denoted $\Gamma_G(i) = \{j : (i,j) \in E\}$, and is the set of all nodes that are directly-connected to i; hence, $k_i = |\Gamma_G(i)|$. The *density* $d(G) = 2m/n(n-1)$ is the number of edges in G relative to the maximum possible number of edges in a graph with n nodes: it ranges from 0 (a set of isolated nodes) to 1 (an *n-complete* graph K_n).

A graph *isomorphism* from a simple graph G to a simple graph H is a bijective mapping $f : V(G) \to V(H)$ such that $(i,j) \in E(G)$ if and only if $(f(i), f(j)) \in E(H)$. We use $G \cong H$ to denote that G and H are isomorphic. A graph *automorphism* is an isomorphism of a graph with itself.[3] A graph $G' = (V', E')$ is a *subgraph* of G if $V' \subseteq V$ and $E' \subseteq E$ where $(i,j) \in E'$ implies that $i, j \in V'$. This definition will not, in general, give a *connected* subgraph. We use $G' \subseteq G$ to denote that G' is a subgraph of G. If $G' \subseteq G$ and $G' \neq G$, then G' is a *proper subgraph* of G, which we write as $G' \subset G$. A *cyclic* (or *acyclic*) subgraph contains some (or no) simple cycles. There are eight 3- and 4-node undirected, connected, and non-isomorphic subgraphs (see Figure 1). We refer to these by $M_a^{(b)}$, where b is the number of nodes in the subgraph, and a is the decimal representation of the smallest binary number derived from the upper triangles of the set of adjacency matrices g corresponding to all isomorphic subgraphs; see Appendix C for details. This notation uniquely represents any b-node subgraph, up to a re-labelling of the nodes.

[insert Figure 1 here]

An n-complete subgraph is also called a *clique*. A *maximal clique* in a graph is a clique that cannot be made any larger by the addition of another node (and its edges) while preserving the complete-connectivity of the clique. A *maximum clique* is a maximal clique with the largest possible number of nodes in the graph, and the *clique number* $w(G)$ is the number of nodes in the maximum clique. Let $G(n,p)$ be an Erdős-Rényi random graph with nodes $V = \{1,\ldots,n\}$ and edges that arise independently with constant probability p. The complete graph K_n, which has all possible edges, is equivalent to $G(n,1)$. A *star* graph $S_{1,n-1}$ has a *center* node i_1 that is directly-connected to every other node (these edges are called *spokes*), and that has no other edges. The *circle* graph C_n has edges $(i, i+1) \in E$ for $i = 1,\ldots,n-1$, and $(1,n) \in E$.

[2] Unless otherwise stated, all summations are computed over the full range of permitted values of the index of summation.

[3] Isomorphic graphs on the same set of nodes have the same topology but will generally have different adjacency matrices, unless they are automorphic, in which case they refer to the *same* graph.

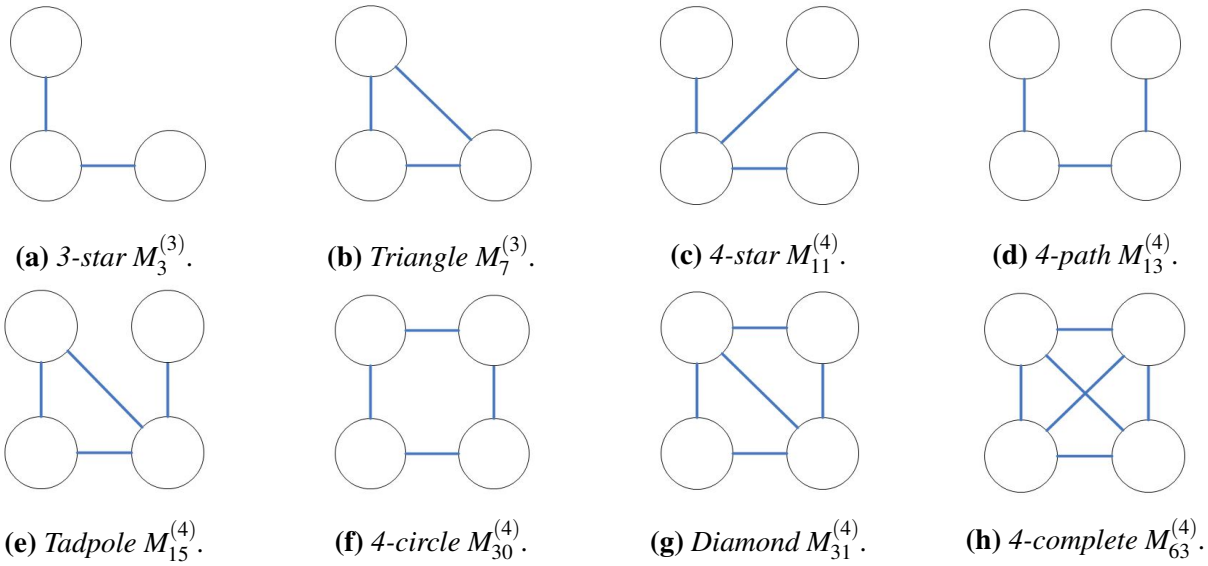

(a) *3-star* $M_3^{(3)}$. **(b)** *Triangle* $M_7^{(3)}$. **(c)** *4-star* $M_{11}^{(4)}$. **(d)** *4-path* $M_{13}^{(4)}$.

(e) *Tadpole* $M_{15}^{(4)}$. **(f)** *4-circle* $M_{30}^{(4)}$. **(g)** *Diamond* $M_{31}^{(4)}$. **(h)** *4-complete* $M_{63}^{(4)}$.

Figure 1: *The eight 3- and 4-node undirected connected subgraphs.*

2.1 Real-World Network Data

Our network data is constructed from the U.S. Department of Transportation's DB1B Airline Origin and Destination survey over the period 1999Q1 to 2013Q4.[4] The source provides quarterly information on a 10% random sample of all tickets that were sold for domestic U.S. airline travel, and has been widely used in the economics literature, e.g., Aguirregabiria and Ho [1], Ciliberto and Tamer [15], Dai et al. [19] and Goolsbee and Syverson [33]. In this paper, we focus on one carrier, Southwest Airlines, which appears in every quarter of the full sample, and is the largest (number of nodes and edges) and densest ($d(G)$) network available in the dataset. We drop any tickets that were sold under a codeshare agreement, or that had unusually high or low fares. We retain coach class tickets, unless more than 75% of the carrier's tickets in a particular quarter were reported as either business or first class, in which case we keep all tickets for that carrier. We aggregate individual tickets to unidirectional route-level observations, and drop routes that have very few passengers, or that do not have a constant number of passengers on each segment. We refer to airports using the official three-letter IATA designators. For full details on the data treatment, see Dossin and Lawford [22]. For each quarter, we build the associated simple unweighted and undirected graph (or "route map") G as follows: (node) the set of nodes V are all airports that served as an origin or destination on some route for Southwest in that quarter; (edges) the set of edges E are all non-directional airport–airport routes for which a sufficient number of passengers bought tickets for direct travel.

[insert Figure 2 here]

Southwest's network has grown steadily over the sample period, from $(n,m) = (54,251)$ in 1999Q1 to $(n,m) = (88,522)$ in 2013Q4. In Figure 2, we give two representations of the 2013Q4 network. The spatial plot shows that passenger activity is highly concentrated between particular geographical areas, creating clearly visible traffic "corridors", while other regions have little or no service. Figure 3 displays some properties of Southwest's network, and the salient features of the numerical data are as follows:

[4]The data is publicly-available, and can be downloaded from `http://www.transtats.bts.gov/`

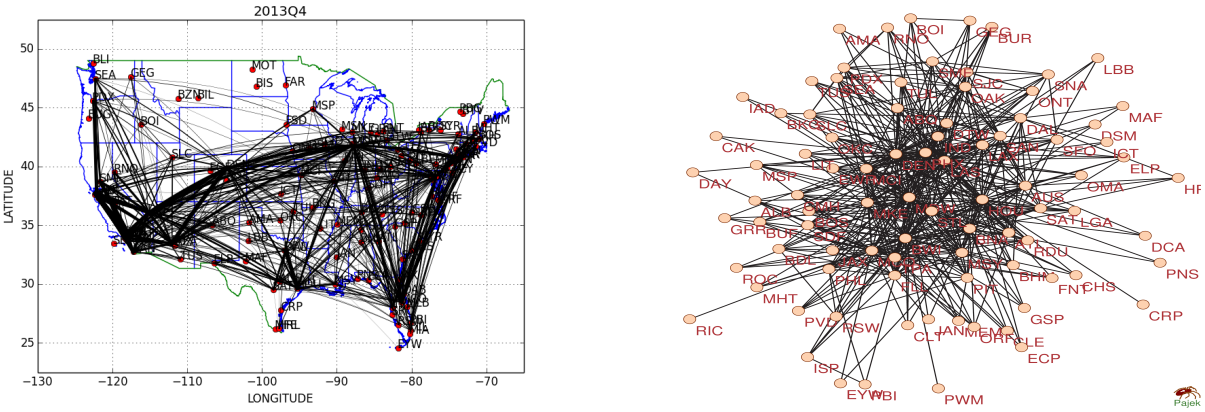

(a) *Spatial network.*

(b) *Topological network.*

Figure 2: *Southwest's network in 2013Q4, computed using nondirectional nonstop round-trip coach class tickets. Routes in (2a) are plotted as minimum-distance paths between directly-connected origin and destination airports; the line width is proportional to the number of passengers on each route, from the U.S. Department of Transportation's Airline Origin and Destination Survey (DB1B). The topological network in (2b) was plotted using Pajek's (Mrvar and Batagelj [52]) Kamada-Kawai visualization algorithm.*

- The number of edges increases almost linearly, while the number of nodes increases slowly until the last two years of the sample, followed by a more rapid increase (Figure 3a).

- The density was stable from 2001 to 2010, at around 0.20, but fell sharply from 2012 onwards, to below 0.14, as the increase in nodes was not matched proportionally by new edges (Figure 3b).

- The diameter and average path length of Southwest's network are, respectively, 3–4 and roughly 2. These values are very close to those of the corresponding $G(n,p)$, when the edge-formation probability p is set equal to the density of Southwest's network.[5] Viewed through this global lens, Southwest's network behaves very much like the random $G(n,p)$ (Figure 3c).

- The overall clustering coefficient measures the fraction of connected triples of nodes that have their third edge connected to form a triangle; the average clustering coefficient computes this measure on a node-by-node basis and then averages across nodes. There is considerably more clustering (both overall and average) in Southwest's network than in the random $G(n,p)$, for which expected overall and average clustering are identical and equal to the density p (Figure 3d).

- Despite the global stability of Southwest's network, displayed by diameter and average path length, there is considerable dynamic variation at the local route level: on average, 2.5% of routes in a quarter were not served in the previous quarter, and 1.2% of routes that were served in the previous quarter were closed in the subsequent one (Figure 3e).

- There is substantial heterogeneity in the *degree centrality* $DC_i = k_i/(n-1)$ across different nodes. We illustrate this with Denver (DEN), Detroit Metropolitan (DTW), Las Vegas McCarran (LAS),

[5] We computed the statistics for $G(n,p)$ using 1,000 replications for each time period, except for expected overall and average clustering, for which we used 100 replications. See Barabási [6] for a non-technical introduction to random graphs.

Chicago Midway (MDW) and Phoenix Sky Harbor (PHX). Midway has experienced several discrete jumps in its activity. Denver entered the network in 2006Q1, with direct links to 8% of other nodes, a figure that rose to a maximum of 72% of other nodes in 2012Q4. Denver and Midway are the two airports that have seen the largest change in degree centrality over the sample period (Figure 3f).

[insert Figure 3 here]

The tendency for many large "sparse" real-world networks to have average path lengths close to those of a random graph but with much higher local clustering (nodes have many mutual neighbours) is called the *small-world* property. Watts and Strogatz [72] give an elegant theoretical explanation for this, and show that the presence of a small number of "short cut" edges, which connect nodes that would otherwise be farther apart than the average path length in a random network, can lead to a rapid fall in average path length, while having very little impact on local clustering.[6] This is consistent with the presence of a small number of high degree "hub" nodes in Southwest's network. For a longer theoretical treatment of the small-world property, with a focus on social networks, see Watts [71].

2.2 Counting Subgraphs

We start by enumerating each of the subgraphs in Figure 1, and separately identify the nodes that make up every occurrence of each subgraph. We make an important distinction here between *nested* and *non-nested* subgraphs. A nested subgraph H' with b nodes and c edges is allowed to be part of a "larger" subgraph H on the same b nodes, in the sense that $H' \subset H$, so that H has more edges than H'. For instance, the tadpole $M_{15}^{(4)}$ can be nested in the diamond $M_{31}^{(4)}$ and the 4-complete $M_{63}^{(4)}$, but not in the 4-star $M_{11}^{(4)}$ or the 4-path $M_{13}^{(4)}$ or the 4-circle $M_{30}^{(4)}$. Conversely, a non-nested subgraph H' cannot be part of any larger subgraph H on the same b nodes, in the above sense. So, the set of all non-nested subgraphs of a given type (e.g., 3-stars) is a subset of all nested subgraphs of the same type (e.g., some 3-stars in a graph might be nested in triangles, while others are not). By definition, the triangle and 4-complete subgraphs cannot be nested. Unless otherwise stated, we assume that a subgraph is nested. We denote non-nested subgraphs by $\widetilde{M}_a^{(b)}$. Throughout the paper, we allow arbitrary overlapping of nodes and edges between two subgraphs (this corresponds to the $\mathscr{F}_1$ "frequency concept" in Schreiber and Schwöbbermeyer [60]).

We count the nested subgraphs (except for $M_{63}^{(4)}$) using the analytic formulae in Proposition 2.1, where $\binom{n}{r}$ is the binomial coefficient, $\mathrm{tr}\,(g)$ is the trace of a square matrix, and $(x)_i$ is the representative element of a vector x. These formulae, and some for subgraphs with more than four nodes, are well known (e.g., Estrada and Knight [26, Section 13.2.5] and Estrada [25, Section 4.4]) and were originally presented by Alon et al. [2, Section 6]. For completeness, we build on the discussion in Estrada and Knight [26] and give a full and intuitive proof of Proposition 2.1 that uses only combinatorial arguments, including the number of closed walks, and the description of more complicated subgraphs in terms of simpler ones (Appendix A), with no explicit mention of moments of the spectral density (the relationship between eigenvalues and structural graph properties is discussed by, e.g., Harary and Schwenk [34]).

[6] Watts and Strogatz [72] define a "sparse" network as one which satisfies, in our notation, $n \gg \frac{m}{n} \gg \log(n) \gg 1$. For Southwest's 2013Q4 network, we have $(n,m) = (88,522)$, whereupon $n = 88 > \frac{m}{n} \approx 5.93 > \log(n) \approx 4.48 > 1$. Throughout, $\log(\cdot)$ refers to the natural log. Wuellner et al. [76, Section II.A] also find evidence that Southwest's network is small-world.

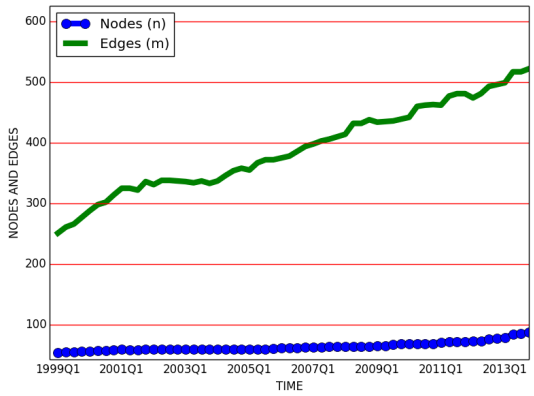

(a) *Number of nodes and edges.*

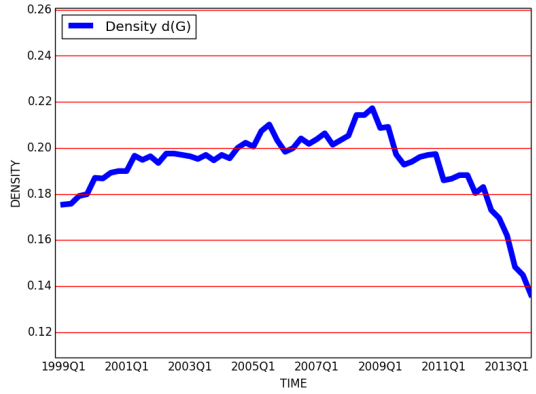

(b) *Density.*

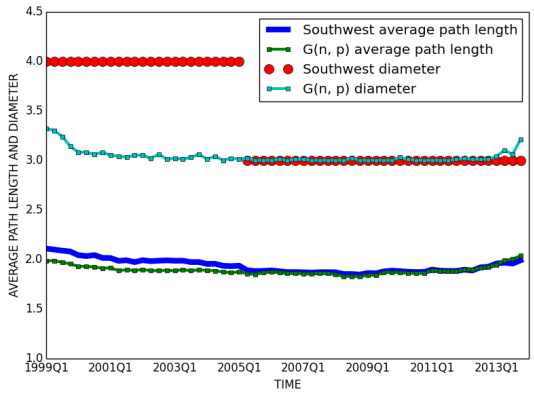

(c) *Diameter and average path length.*

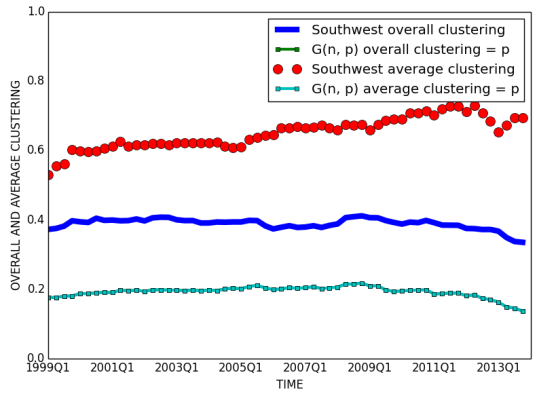

(d) *Overall and average clustering.*

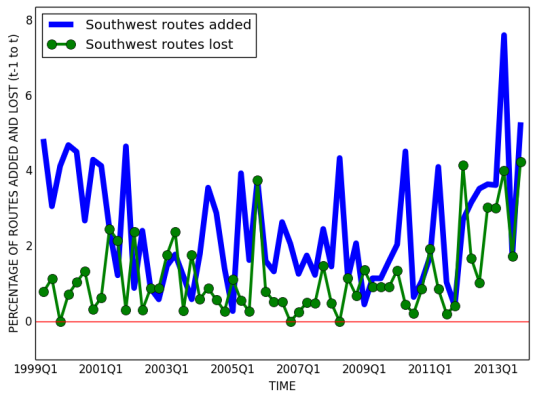

(e) *Percentage of routes added and lost.*

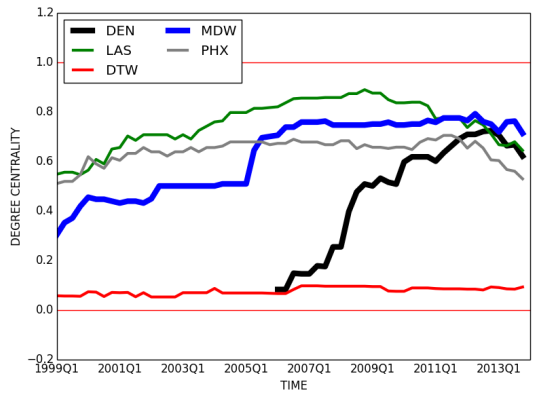

(f) *Degree centrality, selected nodes.*

Figure 3: *Global and local properties of Southwest's network from 1999Q1 to 2013Q4. (3a and 3b) The number of edges (m) increases approximately linearly across the sample period, while the density falls sharply after 2012 due to a rapid increase in the number of new airports (n) that was not matched proportionally by new routes; (3c) the diameter and average shortest path length compared to $G(n, p)$ with density p equal to the density of Southwest's network; (3d) the overall (average) clustering coefficient for Southwest is about two (three) times the clustering of $G(n, p)$; (3e) there is generally a net increase in the number of routes between successive quarters; (3f) heterogeneity in degree centrality over time, for different airports.*

Proposition 2.1 (Analytic formulae for nested subgraph enumeration, Alon et al. [2])**.**

$$|M_3^{(3)}| = \sum_i \binom{k_i}{2} = \frac{1}{2}\sum_i k_i(k_i-1). \tag{1}$$

$$|M_7^{(3)}| = \frac{1}{6}\,\mathrm{tr}\,(g^3). \tag{2}$$

$$|M_{11}^{(4)}| = \sum_i \binom{k_i}{3} = \frac{1}{6}\sum_i k_i(k_i-1)(k_i-2). \tag{3}$$

$$|M_{13}^{(4)}| = \sum_{(i,j)\in E} (k_i-1)(k_j-1) - 3\,|M_7^{(3)}|. \tag{4}$$

$$|M_{15}^{(4)}| = \frac{1}{2}\sum_{k_i>2} (g^3)_{ii}\,(k_i-2). \tag{5}$$

$$|M_{30}^{(4)}| = \frac{1}{8}\,(\mathrm{tr}\,(g^4) - 4\,|M_3^{(3)}| - 2m). \tag{6}$$

$$|M_{31}^{(4)}| = \frac{1}{2}\sum_{i,j} \binom{(g^2)_{ij}\,(g)_{ij}}{2} = \frac{1}{4}\sum_{i,j} ((g^2)_{ij}\,(g)_{ij})\,((g^2)_{ij}\,(g)_{ij}-1). \tag{7}$$

Remark 2.1. Initially, we calculated the 4-complete subgraph count $|M_{63}^{(4)}|$ by brute-force (nested loops). This runs in $O(n^4)$ time but gives us, as a by-product, the set of nodes that make up each 4-complete subgraph (see also Section 2.2.1). However, we can do better than this, and use a simple procedure based on counting the number of triangles in the neighbourhood $\Gamma_G(i)$ of node i. This runs in $O(n^{\omega+1})$ time, where ω is the exponent of matrix multiplication (see Alon et al. [2, p.222]). For instance, using the Coppersmith and Winograd [17] algorithm would give $O(n^{3.376})$.[7] For our dataset, this procedure runs between 20 and 60 times faster than the brute-force count. To summarize (see Appendix A for a proof):

$$|M_{63}^{(4)}| = \frac{1}{24}\sum_i \mathrm{tr}(g_{-i}^3), \tag{8}$$

where g_{-i} is the adjacency matrix corresponding to the subgraph induced by the neighbourhood $\Gamma_G(i)$ of i, and which we denote by $G_- = (V(\Gamma_G(i)), E(\Gamma_G(i)))$; and we use (2) to count the number of triangles.

[insert Table 1 here]

[7] There is a rich and fascinating literature in computer science on fast matrix multiplication, subgraph counting, listing of subgraphs and maximal cliques, and motif detection, with development of exact and approximate algorithms that work well on very large graphs. However, it is not the aim of our paper to provide more efficient routines, or even to use the fastest algorithms that are available, when simpler approaches have good practical runtime performance. For a brief discussion of the history of fast matrix multiplication, see Vassilevska Williams [67, Section 1]. Efficient algorithms for listing all triangles in a graph are given by Björklund et al. [8], while Chu and Cheng [14] develop an exact triangle listing algorithm based on iterative partitioning of the input graph G, and survey other triangle listing algorithms. Vassilevska Williams et al. [68] present fast algorithms for finding some 4-node subgraphs. For a short discussion of the *k-clique problem*, see Vassilevska [66]. Subgraph enumeration on large graphs is discussed by Kashtan et al. [45] and Itzhack et al. [38]. Tran et al. [64], Wong et al. [73] and Khakabimamaghani et al. [46] survey state-of-the-art network motif detection algorithms, and report experimental evidence on the runtime performance of eleven software tools.

Table 1: *Count of 3- and 4-node nested subgraphs in Southwest's 2013Q4 network.*

	Subgraph							
	$M_3^{(3)}$	$M_7^{(3)}$	$M_{11}^{(4)}$	$M_{13}^{(4)}$	$M_{15}^{(4)}$	$M_{30}^{(4)}$	$M_{31}^{(4)}$	$M_{63}^{(4)}$
count	13,457	1,501	176,976	245,533	139,066	24,411	31,584	2,806

In Table 1, we report substantial variation across the number of 3- and 4-node nested subgraphs in 2013Q4. For instance, the counts of the 4-path and triangle (and 4-complete) subgraphs differ by roughly two orders of magnitude. Time series plots of 3- and 4-node nested subgraph counts are given in Figure B.1 in the Appendix: all the subgraph counts increase roughly linearly across the sample, with some small differences in variation around this trend. Note that nested subgraph counts are likely to be correlated, e.g., an additional triangle will increase the nested 3-star count by three. The following result of Fisher and Ryan [29], that we give in a symmetrized form, provides bounds on the number of triangles and 4-complete subgraphs in a simple graph.

Proposition 2.2 (Bounds on number of complete subgraphs, Fisher and Ryan [29])**.** *Let G be a simple graph with clique number $w = w(G)$. For $1 \leq h \leq w$, let T_h be the number of h-complete subgraphs. Then:*

$$\left[\frac{T_{h+1}}{\binom{w}{h+1}}\right]^{\frac{1}{h+1}} \leq \left[\frac{T_h}{\binom{w}{h}}\right]^{\frac{1}{h}}. \tag{9}$$

Remark 2.2. Using our notation, $T_1 = n = 88$ and $T_2 = m = 522$, and it follows from (9) that $m \leq \binom{w}{2}(n/w)^2$ and $|M_7^{(3)}| \leq \binom{w}{3}\left(m/\binom{w}{2}\right)^{3/2}$ and $|M_{63}^{(4)}| \leq \binom{w}{4}\left(|M_7^{(3)}|/\binom{w}{3}\right)^{4/3}$. To illustrate the strength of these inequalities, we used the Bron and Kerbosch [12] algorithm to find all maximal cliques in Southwest's 2013Q4 network: this gives four maximum cliques with $w(G) = 11$.[8] The inequalities reduce to $m \leq 55\,(n/11)^2$ and $|M_7^{(3)}| \leq 165\,(m/55)^{3/2}$ and $|M_{63}^{(4)}| \leq 330\left(|M_7^{(3)}|/165\right)^{4/3}$, which give the rather weak bounds $m \leq 3,520$ and $|M_7^{(3)}| \leq 4,824$ and $|M_{63}^{(4)}| \leq 6,266$, based on the subgraph counts in Table 1.

We count non-nested 3- and 4-node subgraphs using the analytic formulae in Proposition 2.3. It is convenient that each of these is just a linear combination of the nested subgraph count formulae from Proposition 2.1, and so the computational cost is very low. See Appendix A for a proof.

Proposition 2.3 (Analytic formulae for non-nested subgraph enumeration)**.**

$$|\widetilde{M}_3^{(3)}| = |M_3^{(3)}| - 3\,|M_7^{(3)}|. \tag{10}$$

[8] Each of the maximum cliques contains a common 9-complete subgraph, on nodes Nashville (BNA), Baltimore–Washington (BWI), Denver (DEN), Houston William P. Hobby (HOU), Las Vegas McCarran (LAS), Kansas City (MCI), Chicago Midway (MDW), Louis Armstrong New Orleans (MSY) and St. Louis Missouri (STL). The 11-complete subgraphs include, in addition, one of the following pairs of nodes: (FLL, TPA), (LAX, PHX), (MCO, PHX) or (PHX, TPA), on nodes Fort Lauderdale–Hollywood (FLL), Los Angeles (LAX), Orlando (MCO), Phoenix Sky Harbor (PHX), and Tampa (TPA). Each maximum subgraph contains 12.5% of the 88 nodes in the entire 2013Q4 network.

$$|\widetilde{M}_{11}^{(4)}| = |M_{11}^{(4)}| - |M_{15}^{(4)}| + 2\,|M_{31}^{(4)}| - 4\,|M_{63}^{(4)}|. \tag{11}$$

$$|\widetilde{M}_{13}^{(4)}| = |M_{13}^{(4)}| - 2\,|M_{15}^{(4)}| - 4\,|M_{30}^{(4)}| + 6\,|M_{31}^{(4)}| - 12\,|M_{63}^{(4)}|. \tag{12}$$

$$|\widetilde{M}_{15}^{(4)}| = |M_{15}^{(4)}| - 4\,|M_{31}^{(4)}| + 12\,|M_{63}^{(4)}|. \tag{13}$$

$$|\widetilde{M}_{30}^{(4)}| = |M_{30}^{(4)}| - |M_{31}^{(4)}| + 3\,|M_{63}^{(4)}|. \tag{14}$$

$$|\widetilde{M}_{31}^{(4)}| = |M_{31}^{(4)}| - 6\,|M_{63}^{(4)}|. \tag{15}$$

2.2.1 Finding Subgraphs

In many applications, it is useful to list the nodes that make up each individual subgraph. We use brute-force nested loops, with loop indexes chosen to avoid double-counting. The small size of Southwest's network, and of the subgraphs, leads to low runtimes and means that we do not need to use a more sophisticated algorithm. To illustrate, our algorithm for listing all occurrences of the 4-circle runs in $O(n^4)$ time. Choose any node i as the "reference", and let j be the "opposite" node, that is not directly-connected to i. The other two nodes are denoted x and y, and are interchangeable. Loop indexes are chosen so that $i < j$ and $i < x < y$. The approximate run-time $T(n)$ can be found by straightforward but tedious algebra, where we assume that $c = O(1)$ is the constant time needed to check that nodes are distinct and that each edge of the 4-circle is present, and to store the result:

$$\begin{aligned} T(n) &= \sum_{i=1}^{n-3} \sum_{j=i+1}^{n} \sum_{x=i+1}^{n-1} \sum_{y=x+1}^{n} c = c \sum_{i=1}^{n-3} \sum_{j=i+1}^{n} \sum_{x=i+1}^{n-1} (n-x) = \frac{1}{2} c \sum_{i=1}^{n-3} \sum_{j=i+1}^{n} (i-n)(i-n+1) \\ &= -\frac{1}{2} c \sum_{i=1}^{n-3} (i-n)^2 (i-n+1) = \frac{1}{24} c\,(n-3)(3n^3 - n^2 + 6n + 16). \end{aligned} \tag{16}$$

Immediately from (16), the leading term is $T(n) \sim (1/8)\,c\,n^4$. Replacing all of the loop indexes by $1, \ldots, n$ gives a run-time of $T_1(n) = c\,n^4$, with an additional cost in c due to checking for double-counting of subgraphs. Choosing indexes appropriately, based on symmetry and node ordering, gives an observed 8-fold decrease in runtime. The asymptotic approximation is quite accurate: for $n = 88$, and assuming that c is the same for both algorithms, we obtain the ratio $T_1(88)/T(88) \approx 8.31$. We use a similar approach to list all occurrences of each nested and non-nested subgraph. To illustrate, we highlight (Figure 4) the 4-complete subgraph formed in Southwest's 2013Q4 network by the airports Albuquerque (ABQ), Baltimore-Washington (BWI), Denver (DEN) and William P. Hobby, Houston (HOU).

[insert Figure 4 here]

2.3 Scaling Properties

We investigated scaling in subgraph counts as the size of the network increases. Figure B.2 displays log-log plots of the subgraph count against the *number of edges m*, for each of the eight subgraphs in Figure 1, computed on Southwest's network across the 60 quarters in the sample. We superimpose the least squares fit of $\log|M_a^{(b)}|$ on a constant and $\log(m)$. There is a strong scaling relationship for each

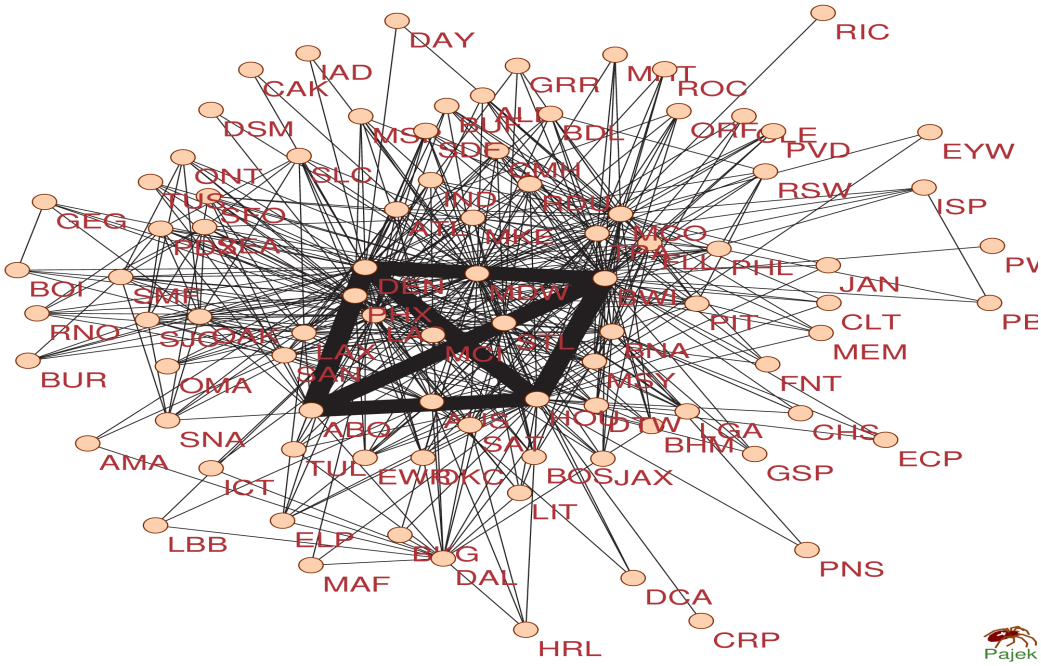

Figure 4: *An illustrative 4-complete subgraph in Southwest's 2013Q4 network (Section 2.2.1).*

of the subgraphs: the estimated slope coefficient and coefficient of determination R^2 from each log-log regression are reported in Table 2. The R^2 is very high in each regression, suggesting that subgraph count and number of edges might be well-approximated by a power-law $|M_a^{(b)}| = Am^\beta$, where A is a constant, and β is the slope coefficient in the log-log regression. Hence, as m increases by a multiplicative factor κ, the subgraph count will increase by a factor κ^β. We would not expect this scaling to arise by tautology.[9]

[insert Table 2 here]

Table 2: *Summary results of log-log regressions of nested subgraph count $|M_a^{(b)}|$ on number of edges m (Figure B.2).*

	Subgraph							
	$M_3^{(3)}$	$M_7^{(3)}$	$M_{11}^{(4)}$	$M_{13}^{(4)}$	$M_{15}^{(4)}$	$M_{30}^{(4)}$	$M_{31}^{(4)}$	$M_{63}^{(4)}$
slope (β)	1.95	1.86	3.17	2.60	2.91	2.87	3.07	3.18
R^2	0.998	0.985	0.993	0.995	0.990	0.984	0.982	0.977

These results lead us to make two observations, which we address in Sections 2.3.1 – 2.3.3:

[9] For excellent surveys of research on empirical power-laws in economics and finance (including firm and city sizes, and CEO compensation), including discussion of theoretical mechanisms (such as random growth) that result in scaling behaviour, and of economic complexity more generally, see Gabaix [30, 31] and Durlauf [23]. Clauset et al. [16] describe power-laws in a variety of real-world datasets, and discuss statistical estimation that can distinguish between power-laws and alternative models. Gabaix et al. [32] present a model of power-law movements in stock prices, and in the volume and number of financial trades.

- It appears that the slope β is closely related to the number of nodes b *in each subgraph*, since $\beta \approx b-1$ in Table 2 (we do not support this statement using statistical inference).
- The scaling seems to hold across a wide range of network sizes (m), but is also robust to the large fall in network density that is observed during the last couple of years of the sample (Figure 3b).

2.3.1 Scaling in Standard Random and Deterministic Models

To start with, is it surprising that there is *any* scaling behaviour in Southwest's network? To build some intuition, consider an independent sequence of Erdős-Rényi random graphs $\{G(n_t,p)\}_{t=1\ldots T}$, where the number of nodes n_t is allowed to vary over time t, but the edge-formation probability $p>0$ is fixed. It is straightforward to find the expected nested subgraph counts for 3- and 4-node subgraphs in $G(n,p)$, and these well-known results are reported in Proposition 2.4, with the leading term of the asymptotic (large n) expansion; for completeness, a proof is given in Appendix A. The expectation operator is denoted by $\mathrm{E}(\cdot)$.

Proposition 2.4 (Analytic formulae for nested expected subgraph counts in $G(n,p)$)**.**

$$\mathrm{E}(|M_3^{(3)}|) = 3\binom{n}{3}p^2 \sim \frac{1}{2}n^3p^2.$$

$$\mathrm{E}(|M_7^{(3)}|) = \binom{n}{3}p^3 \sim \frac{1}{6}n^3p^3.$$

$$\mathrm{E}(|M_{11}^{(4)}|) = 4\binom{n}{4}p^3 \sim \frac{1}{6}n^4p^3.$$

$$\mathrm{E}(|M_{13}^{(4)}|) = 12\binom{n}{4}p^3 \sim \frac{1}{2}n^4p^3.$$

$$\mathrm{E}(|M_{15}^{(4)}|) = 3\binom{n}{3}(n-3)p^4 \sim \frac{1}{2}n^4p^4.$$

$$\mathrm{E}(|M_{30}^{(4)}|) = 3\binom{n}{4}p^4 \sim \frac{1}{8}n^4p^4.$$

$$\mathrm{E}(|M_{31}^{(4)}|) = 6\binom{n}{4}p^5 \sim \frac{1}{4}n^4p^5.$$

$$\mathrm{E}(|M_{63}^{(4)}|) = \binom{n}{4}p^6 \sim \frac{1}{24}n^4p^6.$$

Remark 2.3. It is easy to derive analytic formulae for expected non-nested subgraph counts in $G(n,p)$, by multiplying each equation in Proposition 2.4 by $(1-p)^{b(b-1)/2-c}$, where the number of edges c in the subgraph is the power on p, and b is the number of nodes in the subgraph.

Consider the slope coefficient β that would be implied by $\{G(n_t,p)\}_{t=1\ldots T}$, using triangle subgraphs $M_7^{(3)}$ for illustration. From Proposition 2.4, $\mathrm{E}(|M_7^{(3)}|) \sim \frac{1}{6}n^3p^3$. Further, $\mathrm{E}(m) = \binom{n}{2}p \sim \frac{1}{2}n^2p$ in an Erdős-Rényi graph and so $n \sim (2/p)^{1/2}(\mathrm{E}(m))^{1/2}$. It follows that $\mathrm{E}(|M_7^{(3)}|) \sim (2/9)^{1/2}p^{3/2}(\mathrm{E}(m))^{3/2}$, which implies that $\beta = 1.5$. By the same argument, the implied slope coefficient equals 1.5 for all

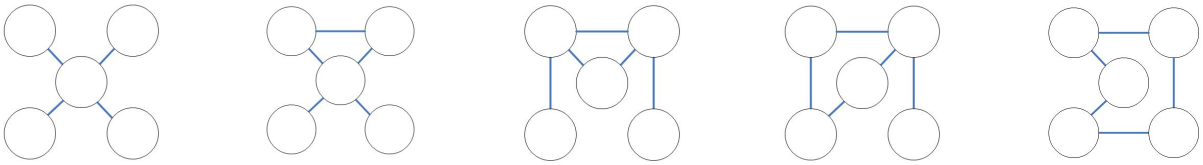

(a) *5-star* $M_{75}^{(5)}$. **(b)** *Cricket* $M_{79}^{(5)}$. **(c)** *Bull* $M_{87}^{(5)}$. **(d)** *Banner* $M_{94}^{(5)}$. **(e)** *5-circle* $M_{236}^{(5)}$.

Figure 5: *A selection of 5-node undirected connected subgraphs.*

3-node subgraphs, and equals 2 for all 4-node subgraphs, and in general equals $b/2$ for all b-node subgraphs in $\{G(n_t,p)\}_{t=1...T}$. This shows that scaling behaviour can arise in classical random models. In fact, Itzkovitz and Alon [39, equation (7)] report a general scaling result for the count of a nested subgraph, with b nodes and c edges, in an Erdős-Rényi graph with n nodes and expected degree $\mathrm{E}(k)$ as: $\mathrm{E}(|M_a^{(b)}|) \sim n^{b-c}(\mathrm{E}(k))^c$. Since $\mathrm{E}(k) = (n-1)p$ in Erdős-Rényi, we have $\mathrm{E}(|M_a^{(b)}|) \sim n^b p^c$ as $n \to \infty$, and using $n \sim (2/p)^{1/2}(\mathrm{E}(m))^{1/2}$, this gives $\log(\mathrm{E}(|M_a^{(b)}|)) \sim \text{constant} + \frac{b}{2}\log(\mathrm{E}(m))$.

As a second example, let us take the deterministic dynamic model $\{S_{1,n_t-1}\}_{t=1,...,T}$ based upon the n-star, with $n_t = t$, and count the number of b-star subgraphs. Since $m = n-1$, we have from Proposition 2.1 that (3-star) $|M_3^{(3)}| \sim (1/2)m^2$ and (4-star) $|M_{11}^{(4)}| \sim (1/6)m^3$, with implied slopes of 2 and 3 respectively. In general, the number of b-star subgraphs in the n-star equals

$$\binom{n-1}{b-1} \sim \frac{n^{b-1}}{(b-1)!} \sim \frac{m^{b-1}}{(b-1)!},$$

with implied slope $b-1$. While it is tempting to conjecture that β always increases in the number of nodes b in the subgraph, an easy counterexample shows that this is not true in general. Take the deterministic model $\{C_{n_t}\}_{t=1,...,T}$ based on the n-circle, with $n_t = t$. Since $k_i = 2$ for all i, we see that (3-star) $|M_3^{(3)}| = n = m$, with implied slope β equal to 1. However, there are *no* b-star subgraphs in the n-circle, and the implied slope β equals 0, for any $b > 3$; there will be no triangles $M_7^{(3)}$ in any n-circle.

2.3.2 Further Evidence on Scaling in Southwest's Network

Nevertheless, we do observe a possible power-law scaling in Southwest's network, with a slope that increases in b. To provide further evidence, we also examined five 5-node subgraphs for which analytic nested count formulae are available in Estrada and Knight [26], and a single 6-node subgraph, the 6-star $M_{1099}^{(6)}$. The 5-node subgraphs are displayed in Figure 5: they are the 5-star, the cricket, the bull, the banner (or flag) and the 5-circle. Log-log plots appear in Figure B.3 in the Appendix, with results in Table 3.

[insert Figure 5 here]

[insert Table 3 here]

There is some evidence that 5-node subgraphs have a scaling slope of $\beta \approx 4$, although the slope for the 6-star seems to be closer to 6 than to 5. We can suggest that Southwest's network and dynamics are such that the log-log scaling will be approximately $\beta \approx b-1$, at least for subgraphs of size $b = 3,4,5$.

Table 3: *Summary results of log-log regressions of nested subgraph count $|M_a^{(b)}|$ on number of edges m (Figure B.3).*

	Subgraph					
	$M_{75}^{(5)}$	$M_{79}^{(5)}$	$M_{87}^{(5)}$	$M_{94}^{(5)}$	$M_{236}^{(5)}$	$M_{1099}^{(6)}$
slope (β)	4.44	4.12	3.88	3.96	3.69	5.70
R^2	0.987	0.988	0.990	0.990	0.981	0.981

While a general proof of conditions under which this sort of behaviour can arise is beyond the scope of this paper, a heuristic argument for the 3-star in a general network proceeds as follows:

$$|M_3^{(3)}| = \frac{1}{2}\sum_i k_i(k_i-1) = \frac{n}{2}\left(\mathrm{E}(k^2)-\mathrm{E}(k)\right). \tag{17}$$

If we assume that the mean of the degree distribution is bounded and that the variance increases linearly with n, i.e., $\mathrm{E}(k) = O(1)$ and $\mathrm{var}(k) = O(n)$, so that $\mathrm{E}(k^2) = O(n)$, then it follows immediately from (17) that $|M_3^{(3)}| = O(n^2)$.[10] As a network grows (n to $n+1$), at least one edge, and no more than n edges, must be added for every new node if the network is to remain connected, and so we can suppose that $n \sim c(\alpha)m^\alpha$ for $1/2 \leq \alpha \leq 1$, where $c(\alpha)$ is a constant. Then, $|M_3^{(3)}| = O(m^\beta)$, with $\beta = 2\alpha \leq 2$. Simple conditions on (a) the first two moments of the degree distribution $P(k)$, and (b) the relationship between m and n, would be sufficient to give the observed scaling behaviour for the 3-star in Southwest's network.

It seems that any scaling behaviour might generally depend upon (i) the number of nodes b in the subgraph, (ii) the topology of the subgraph for a given b (e.g., the 3-star or the triangle), (iii) the nature of the graph G in which these subgraphs are contained, and (iv) the way in which the topology of G evolves as n increases. We could expect to find $\beta \approx b-1$ in some other real-world networks of interest.

2.3.3 Robustness of Scaling Behaviour to Changes in Network Evolution

We now focus on the observation that the scaling in Figures B.2 and B.3 appears to be robust to a significant change in network evolution: in 2012 and 2013, the net number of routes increased at a much slower rate, relative to the net number of airports, than it did before 2012, with a resulting fall in network density (Figure 3b). We obtain analytic results for a toy regime-switching model of network evolution, and show how apparently robust scaling can appear, despite significant underlying changes in the dynamics.

Consider a deterministic dynamic network model that starts with two connected nodes and adds one additional node in each subsequent time period. There are two regimes, where l is the total number of nodes in the network in a given time period:

- (**Regime 1**) For $l \leq n^\star$, the network evolves as an n-star. One of the initial two nodes is chosen to be the (fixed) center, and each subsequent node links only to the center node.
- (**Regime 2**) For $l > n^\star$, each subsequent node links to *all* existing nodes.

[10] For instance, the n-star has $\mathrm{E}(k) = 2-2/n = O(1)$ and $\mathrm{E}(k^2) = n-1 = O(n)$ and $\mathrm{var}(k) = n-5+8/n-4/n^2 = O(n)$.

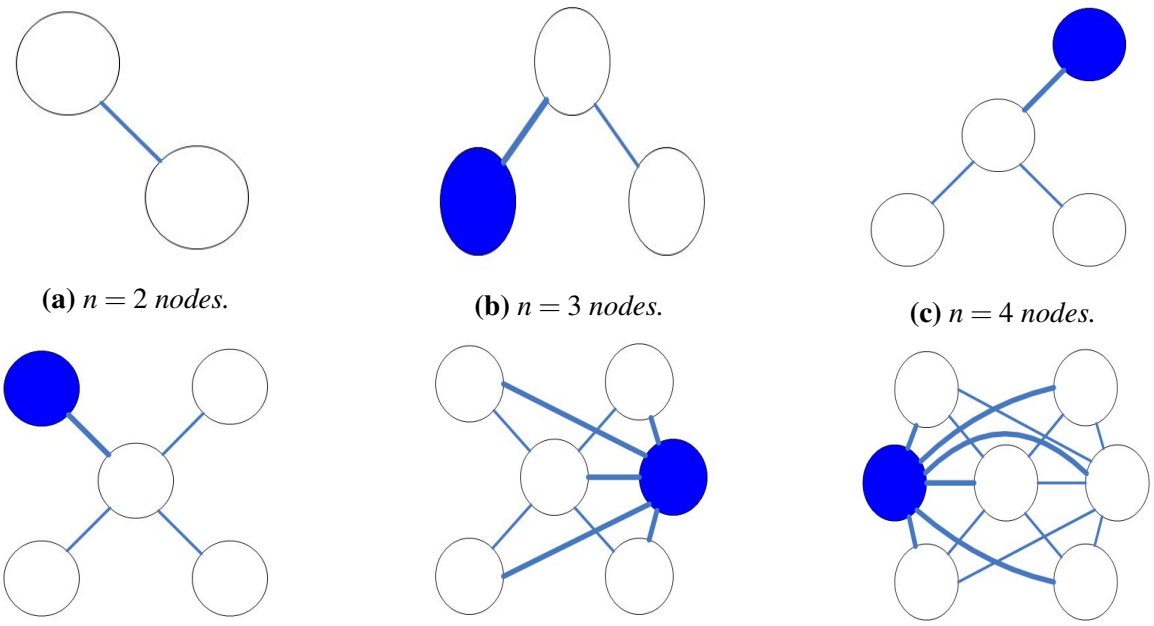

(a) $n = 2$ *nodes.* **(b)** $n = 3$ *nodes.* **(c)** $n = 4$ *nodes.*

(d) $n = n^\star = 5$ *nodes.* **(e)** $n = 6$ *nodes.* **(f)** $n = 7$ *nodes.*

Figure 6: *Toy regime-switching model, with regime change after $n^\star = 5$ (Section 2.3.3). In each step, the new node and new edges are highlighted in bold.*

So, $n^\star$ is the network size at which the model of evolution switches from Regime 1 to Regime 2. The network will evolve as an n-star for $n \leq n^\star$ and will, intuitively, become increasingly like a complete graph as $n > n^\star$ and n becomes large. See Figure 6 for an illustration, with $n^\star = 5$.

[insert Figure 6 here]

Let us consider the number of 3-stars in the combined network described by Regimes 1 and 2.

- (**Regime 1**) Here, $l = 2, 3, \ldots, n^\star$ and $m = l - 1$. From (1), the number of nested 3-stars is given by $|M_3^{(3)}| = \binom{m}{2} = \frac{1}{2}m(m-1) \sim \frac{1}{2}m^2$ as $n^\star$ increases.
- (**Regime 2**) Here, $l = n^\star + 1, n^\star + 2, \ldots, n$. When $l = n^\star + 1$, we obtain $m = (n^\star - 1) + n^\star = 2n^\star - 1$. When $l = n^\star + 2$, we have $m = (n^\star - 1) + n^\star + (n^\star + 1) = 3n^\star$. In general, and setting $a = l - n^\star$, we can show that the number of edges is given by

$$m = (a+1)n^\star + \sum_{j=-1}^{a-1} j = (a+1)n^\star + \sum_{j=1}^{a+1}(j-2) = (a+1)\left(n^\star + \frac{a}{2} - 1\right),$$

and so $m \sim \frac{1}{2}a^2$ as a becomes large (so that $n >> n^\star$). From (1), the nested 3-star count is $|M_3^{(3)}| = \frac{1}{2}\sum_{k \in D} k(k-1)$. In Regime 1, $D = \{1, 1, \ldots, 1, l-1\}$, where $l-1$ nodes have degree 1. In Regime 2, $D = \{(a+1), \ldots, (a+1), (n^\star + a - 1), \ldots, (n^\star + a - 1)\}$, where $n^\star - 1$ nodes have

degree $a+1$, and $a+1$ nodes have degree $n^\star+a-1$. Putting these elements together, it follows that

$$|M_3^{(3)}| = \frac{1}{2}(a+1)\left(a(n^\star-1)+(n^\star+a-1)(n^\star+a-2)\right) \sim \frac{1}{2}a^3,$$

as a becomes large. Using $m \sim \frac{1}{2}a^2$ and $|M_3^{(3)}| \sim \frac{1}{2}a^3$, we have $|M_3^{(3)}| \sim 2^{1/2}m^{3/2}$ in Regime 2.

Hence, there will be a transition in the implied scaling slope β as the regime changes, from 2 in Regime 1 (if $n^\star$ is large) to 1.5 in Regime 2 (if n is large relative to $n^\star$). Although there is a different degree of scaling in each regime, and a very different model of evolution, if we ignore the switch and apply least squares to the entire sample ($l = 1,\ldots,n$) then the regression slope will be a weighted average of the slopes in the individual regimes.[11] It is possible that Southwest's network evolution changed substantially between 2011 and 2012, and that the regressions are averaging the scaling in two or more regimes. Indeed, the regression errors (Figures B.2 and B.3) do seem consistently larger at the end (and start) of the sample, when n is largest (smallest).

2.3.4 Does Constant-Slope log-log Scaling Hold for all m?

We use Proposition 2.2 to show that the constant-slope log-log scaling implied by Tables 2 and 3 cannot hold for all m, *in the case of the triangle and 4-complete subgraphs*. This suggests that the scaling is unlikely to hold for all m for the other 3- and 4-node subgraphs either. Consider the triangle. From (9),

$$\log|M_7^{(3)}| \leq \log\binom{w}{3} - \frac{3}{2}\log\binom{w}{2} + \frac{3}{2}\log(m),$$

where w is the clique number. Since $w \geq 2$ in a connected graph G if $m \geq 2$, we can rewrite this as

$$\log|M_7^{(3)}| \leq \log(w-2) - \frac{1}{2}\log\left(\frac{9}{2}(w-1)w\right) + \frac{3}{2}\log(m).$$

Define $C(w) = \log(w-2) - \frac{1}{2}\log\left(\frac{9}{2}(w-1)w\right)$. Figure B.2b gives a log-log scaling $\log|M_7^{(3)}| = \alpha + \beta\log(m)$, where $\alpha \approx -4.18$ and $\beta \approx 1.86$. This constant scaling can only hold for all m if $C(w) + \frac{3}{2}\log(m) \geq \alpha + \beta\log(m)$, so that $C(w) - \alpha \geq \left(\beta - \frac{3}{2}\right)\log(m)$ for all m. Given $\beta \approx 1.86$, the right-hand-side is strictly positive and increasing in m. Consider two cases: (1) If w is constant in m (say, $w = 11$) then $C(w) - \alpha$ is also constant in m, and the inequality will fail for some m; (2) Instead, let $C(w)$ increase in m. As m increases, there will be a point at which n can increase by at most $O(m)$.[12] By definition, $w \leq n$ and so $w = O(m)$. In that case, $\lim_{m\to\infty} C(w(m)) = -\frac{1}{2}\log\left(\frac{9}{2}\right) \approx -0.75$. For all $w \geq 2$, $C(w) < 0$ and so, at some point, the right-hand-side $\left(\beta - \frac{3}{2}\right)\log(m)$ will exceed $C(w) - \alpha$ for *any* connected graph G. Therefore, the constant-slope log-log linear scaling cannot hold for all m. This argument goes through, with minor modifications, for the 4-complete subgraph, i.e., $C(w) - \alpha \geq (\beta - 2)\log(m)$ from (9), where $C(w) = \log\binom{w}{4} - 2\log\binom{w}{2} = \log(w-3) + \log(w-2) - \log(6(w-1)w)$, with $\alpha \approx -11.66$ and $\beta \approx 3.18$ from Figure B.2h; and noting that $\lim_{m\to\infty} C(w(m)) = -\log(6) \approx -1.79$.

[11] In Figure B.4 we illustrate the toy model using simulated data, with $l = 4,\ldots,n^\star = 20,\ldots,n = 30$: the slopes of 2 (in Regime 1) and 1.5 (in Regime 2) are averaged by the regression to 1.56 (with a very high R^2 of 0.983).

[12] An n-star and an n-path have $m = n-1$ and $n = m+1$; for a complete graph, $m = \frac{1}{2}n(n-1)$ and $n = \frac{1}{2}(1+\sqrt{8m+1})$.

2.4 Which Subgraphs are Motifs?

Do any subgraphs arise more (or less) often than we would expect at random? We considered the significance of non-nested subgraph counts against two randomized null networks, to detect: (a) 3-node motifs relative to $G(n,p)$ (Section 2.4.1), (b) 3-node motifs relative to a degree-preserving rewiring of the original network (Section 2.4.2), and (c) 4-node motifs relative to a distribution that controls for the number of 3-node non-nested subgraphs in the network, following Milo et al. [51] (Section 2.4.3). It is well known that the choice of null distribution is of critical importance, and will affect which subgraphs are identified as motifs. Certainly, the null should have some of the properties of the real-world network.[13] It is also important to search for *non-nested* rather than nested subgraph motifs, for two reasons. First, nested 3-star and 4-star subgraph counts depend only on the first few moments of $P(k)$, from (17) and

$$|M_{11}^{(4)}| = \frac{n}{6}\left(\mathrm{E}(k^3) - 3\,\mathrm{E}(k^2) + 2\,\mathrm{E}(k)\right),$$

which follows from (3). So, both $|M_7^{(3)}|$ and $|M_{11}^{(4)}|$ will be invariant to a degree-preserving rewiring, and we will not be able to use this approach to find nested b-star motifs in general. Second, since an individual motif is interpreted as a particular (unique) topology on a given b nodes, it makes intuitive sense to look for non-nested subgraphs, and this is typical in the literature: a given set of nodes form a motif (or anti-motif) when they do not have any more complicated topological interrelationship, and their topology is statistically overrepresented (or underrepresented) in the network. We perform inference using the z-score of each subgraph count.

2.4.1 3-Node Motifs Relative to $G(n,p)$

A result of Ruciński [58, Theorem 2] gives the asymptotic distribution of the z-score relative to $G(n,p)$:

Theorem 2.5 (Asymptotic normality of the z-score, Ruciński [58])**.** *Let $J(n,p)$ be a random graph with nodes $V = \{1,\ldots,n\}$ and edges that arise independently with probability $p(n)$. Let X_n denote the count of subgraphs of $J(n,p)$ that are isomorphic to a graph G. Define $\gamma = \max\{|E(G')|/|V(G')| : G' \subseteq G\}$, and let $\mathrm{E}(X)$ and $\mathrm{var}(X)$ be the expectation and variance of a random variable X. Then,*

$$Z_n = \frac{X_n - \mathrm{E}(X_n)}{\sqrt{\mathrm{var}(X_n)}} \xrightarrow{d} \mathrm{N}(0,1),$$

as $n \to \infty$, if and only if $n\,(p(n))^{\gamma} \to \infty$ and $n^2(1-p(n)) \to \infty$; and $\mathrm{N}(0,1)$ is the standard normal.

Remark 2.4. We do not require the full strength of the result. When $p = p(n)$ is constant in n, $J(n,p)$ reduces to $G(n,p)$. Note that γ is one half of the largest average degree across all subgraphs G' of G (which may arise for G itself). For the eight subgraphs in Figure 1, it is easy to see that $\gamma > 0$, and that $n\,p^{\gamma} \to \infty$ if $p \neq 0$, and $n^2(1-p) \to \infty$ if $p \neq 1$. When $p = 0$ (set of isolated nodes) or $p = 1$ (complete graph), there is no variation in the subgraph count, and the result does not hold.

[13] See Itzkovitz et al. [40, Appendix A] for some discussion of randomized ensembles subject to constraints. We also experimented with variants of the *erased configuration model*, with and without some clustering (e.g., Angel et al. [4], Newman [54], Schlauch and Zweig [59]), but found that these gave some self-loops and many multiple-edges. Since our networks are quite small, we cannot make use of the observation that these issues are not important asymptotically, and the resulting randomized graphs have rather different properties to the real-world networks.

We compute the expected number of subgraphs in $G(n,p)$ using Proposition 2.4, modified for non-nested subgraphs. We simulate the variance of the count by 1,000 replications from $G(n,p)$, with edge-probability p set equal to the density $d(G)$ of the real network.[14] For each quarter in the full sample, we compute the z-score for the non-nested 3-star and the triangle (Figure 7); we include the z-score for the *nested* 3-star for reference. It is only strictly correct to search for 3-node motifs since the $G(n,p)$ only matches the number of 1- and 2-node subgraphs (nodes and expected edges) in the real-world network. We observe that (a) the z-scores increase over time, which corresponds to a general increase in the size of the network (n), and they are correlated across subgraphs, (b) the nested 3-star is highly significant in every period, which might lead us to conclude (incorrectly) that the non-nested 3-star is a motif too — this shows the importance of searching for non-nested motifs, (c) the triangle is a motif across the full sample, and (d) the non-nested 3-star is a motif from 2003 onwards.[15] We can interpret these results as follows:

- There is more clustering (triangles) than in $G(n,p)$, and this increases over time. While clustering coefficients indicate the higher clustering, they do not clearly show the dynamic increase relative to $G(n,p)$ that is suggested by the triangle motif (Figure 3d).
- There are more "spokes" (non-nested 3-stars) than in $G(n,p)$, from 2003 onwards. Nevertheless, Southwest's network has similar average path lengths to a random network (Figure 3c).

[insert Figure 7 here]

While some authors, e.g., Prill et al. [56], consider motifs relative to $G(n,p)$, this null only matches the number of nodes and expected edges, and so we now also match the degree distribution $P(k)$ of the real-world network. Theorem 2.5 no longer applies, and the asymptotic distribution of the z-score is not generally known, so we use bootstrap p-values to assess statistical significance.

2.4.2 3-Node Motifs Relative to a Degree-Preserving Rewiring

In Figure B.5, we plot the degree distributions of Southwest's network (kernel density estimates) and the corresponding $G(n,p)$. While $G(n,p)$ matches n and the density $d(G)$ of the real-world network, it cannot generate realizations that capture the "hub-and-spoke" nature of the observed degree distribution $P(k)$. In this section, we use a null distribution that matches $P(k)$, by a Markov-chain degree-preserving rewiring of G. Starting from the observed network G, we select one pair of edges $(x_1,y_1) \in E$ and $(x_2,y_2) \in E$ at random, such that the nodes are all distinct, and both $(x_1,y_2) \notin E$ and $(x_2,y_1) \notin E$. Then, edges (x_1,y_1) and (x_2,y_2) are replaced by edges (x_1,y_2) and (x_2,y_1). The edge-switching is repeated until G has been sufficiently randomized.

The resulting graph will have the same number of nodes n and edges m as the original graph, and the same degree distribution $P(k)$ but, in general, a *different* topology. In Figure 8, we plot the z-scores of the non-nested 3-star and the triangle. Normal and bootstrap p-values give similar results, and so we refer to the $\mathrm{N}(0,1)$ critical values. The results are strikingly different to those for $G(n,p)$ in Figure 7. We see that:

[14] We discard any realizations of $G(n,p)$ that are not connected.

[15] Itzkovitz and Alon [39] study the occurrence of subgraphs in geometric network models, with nodes arranged on a lattice, and edges arising at random with a probability that decreases in the distance between nodes. Relative to Erdős-Rényi, they show that all subgraphs with at least as many edges as nodes (in the subgraph) will be motifs as $n \to \infty$, if the real-world and Erdős-Rényi networks have the same expected degree $\mathrm{E}(k)$. They give a similar result for heavy-tailed random networks.

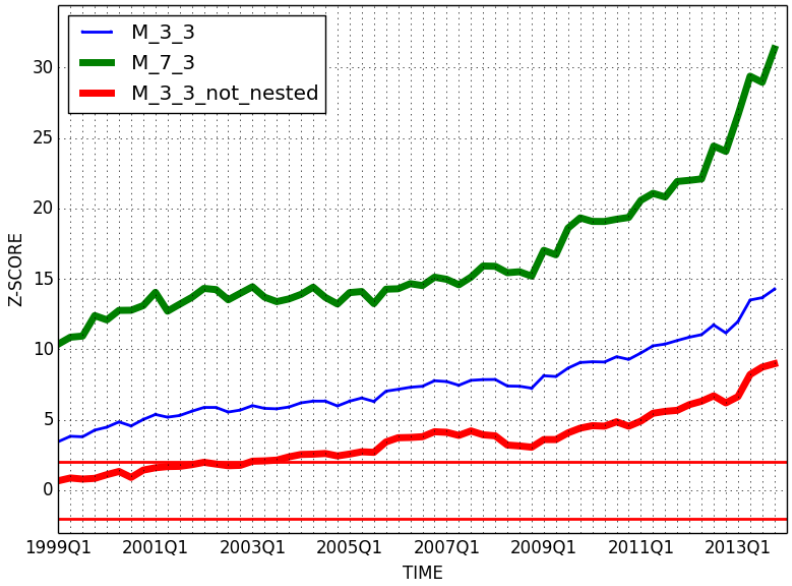

Figure 7: *The z-scores for the nested (thin line) and non-nested 3-star, and the triangle, relative to $G(n,p)$. The mean subgraph counts are computed using the analytic formulae of Proposition 2.4, with modification for non-nested subgraphs. The variance of each subgraph count is computed numerically, by 1,000 draws from $G(n,p)$. The horizontal red lines represent the approximate 95% critical values, ± 2. (Section 2.4.1)*

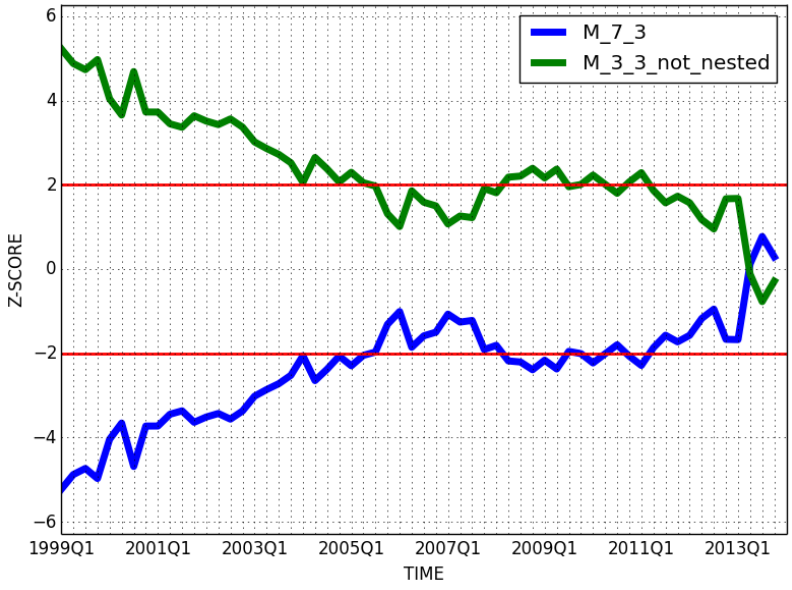

Figure 8: *The z-scores for the non-nested 3-star and triangle, relative to a degree-preserving rewiring of the real-world network G. The mean and variance of the subgraph count are computed numerically, by 1,000 draws from the randomized ensemble. Bootstrap p-values are used for inference, with 100 bootstrap replications. Since bootstrap and standard normal p-values are similar, we refer to the horizontal red lines, which represent the approximate 95% critical values, ± 2. (Section 2.4.2)*

- The non-nested 3-star is a motif from 1999 – 2005 and again from 2008 – 2011; it has become notably less significant from 2012 onwards.

- The triangle has exactly the opposite interpretation, as an anti-motif. This follows by construction: comparing the z-score (z_1) of $|\widetilde{M}_3^{(3)}|$ and the z-score (z_2) of $|M_7^{(3)}|$, and using $|\widetilde{M}_3^{(3)}| = |M_3^{(3)}| - 3\,|M_7^{(3)}|$ from (10), and the fact that $|M_3^{(3)}|$ is invariant to rewiring, which gives $\mathrm{E}(|M_3^{(3)}|) = |M_3^{(3)}|$ and $\mathrm{var}(|M_3^{(3)}|) = 0$, it is easy to see that $z_1 = -z_2$. Hence, if one of these subgraphs is a motif, then the other will be an anti-motif; however, both subgraphs can be insignificant (not motifs) together.

[insert Figure 8 here]

Together, these results tell us that triangles (clustering) have become much more prevalent over time, while the importance of 3-stars (spokes) has decreased. This is somewhat surprising given the fall in network density over the same period (Figure 3b). So far, we have not discussed 4-node subgraphs (motifs), since there might be a large number of 4-node subgraphs simply because there is an "excessive" number of 3-node subgraphs in the network. In the next section, we search for 4-node motifs, controlling for the number of 1-, 2- and 3-node non-nested subgraphs.

2.4.3 4-Node Motifs Relative to a Degree-Preserving Rewiring that Controls for 3-Node Non-Nested Subgraphs

The null distribution is generated as follows, starting from the observed graph G. We first perform a degree-preserving rewiring as described in Section 2.4.2, until a "sufficient" degree of randomness has been attained. We then use simulated annealing (Eglese [24]), with successive edge-pair switches, to match the number of 3-node non-nested subgraphs to those in the original graph G. Simulated annealing attempts to avoid local optima by sometimes accepting a rewiring which increases the value of the optimization function.[16] In Figure 9, we plot the z-score for each 4-node non-nested subgraph. We observe that:

- The non-nested 4-star is a strong motif for most of the sample, although it becomes less significant.

- The non-nested 4-circle and diamond are borderline motifs for much of the sample (2002 – 2013).

- The non-nested 4-path and tadpole are strong anti-motifs for the entire sample.

- The 4-complete was an anti-motif over 1999 – 2006 but has become progressively more significant since then, and was a borderline motif in 2013.

[insert Figure 9 here]

[16] Specifically, we minimize the function $\text{Energy} = \sum_i |(\theta_{\text{real}})_i - (\theta_{\text{rand}})_i| \big/ ((\theta_{\text{real}})_i + (\theta_{\text{rand}})_i)$, by performing edge-pair switches on the already randomized graph, where the non-nested 3-node subgraph counts in the real and randomized (rand) data are given by $\theta_\cdot = (|\widetilde{M}_3^{(3)}|, |M_7^{(3)}|)^\intercal$. In our notation, we suppress the dependence of Energy and $\theta_\cdot$ on the current "time" t spent in the optimization. We define the slowly-decaying *temperature* function $\Psi(t+1) = \Psi(t)/\log(t+1)$, with initial value $\Psi(1) = 100$. At each time step, a random edge-switch is always accepted if it reduces the current Energy, and is otherwise accepted with probability $e^{-|\Delta\text{Energy}|/\Psi(t)}$, where ΔEnergy is the difference in Energy before and after the edge-switch. One edge-switch is performed at each temperature level, and the stopping criterion is achieved when Energy < 0.00001.

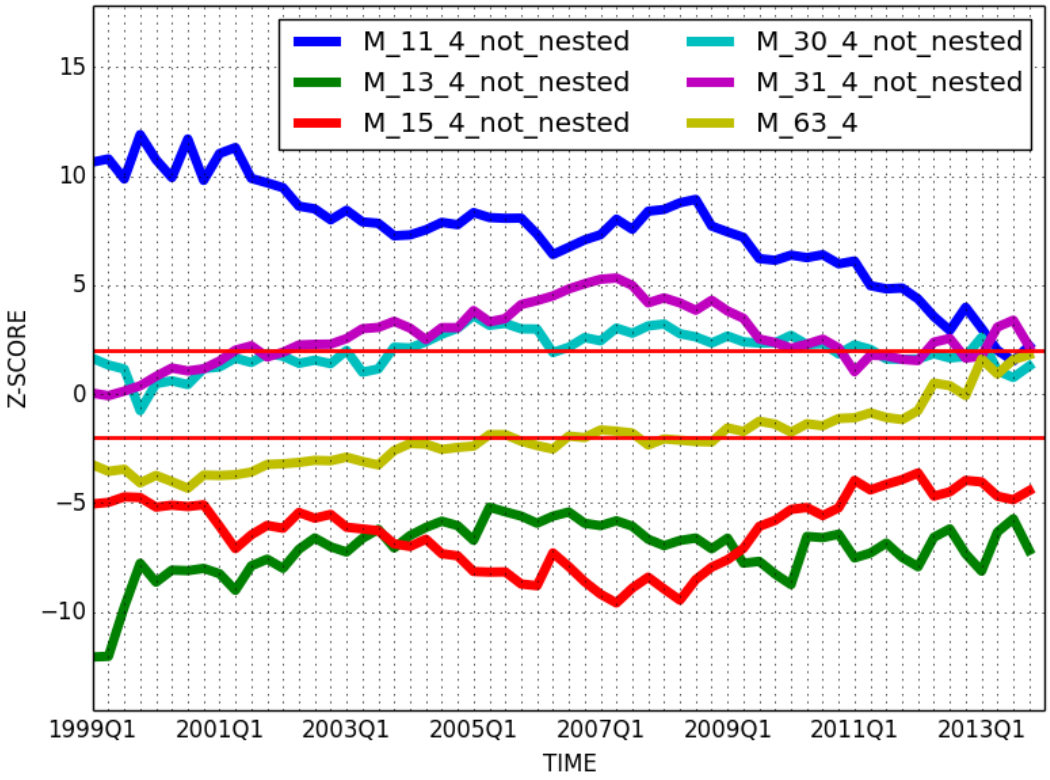

Figure 9: *The z-scores for the non-nested 4-star, 4-path, tadpole, 4-circle, diamond and 4-complete subgraphs, relative to a degree-preserving rewiring of the real-world network G, followed by a simulated annealing optimization that matches the number of non-nested 3-node subgraphs in G, in every time period. The mean and variance of the subgraph counts are computed numerically by 1,000 draws from the randomized ensemble. Bootstrap p-values are used for inference, with 100 bootstrap replications. Since bootstrap and normal p-values are similar, we refer to the horizontal red lines, which represent the approximate 95% critical values, ± 2. (Section 2.4.3)*

These results suggest that the importance of spoke airports (4-star) in Southwest's network has fallen over time — consistent with the findings of Section 2.4.2, while clustered groups of airports (diamond and 4-complete) have gained or maintained a level of importance. In particular, the rise of the 4-complete subgraph implies that new routes have completed groups of airports that were not previously completely-connected, and gives us some new insight into the decision-making that underlies network evolution. The significance of the 4-circle is rather unexpected, since travel between two opposite "corners" requires a two-step trip. The underrepresentation of the tadpole and 4-path makes sense, since both patterns imply two-step or even three-step trips between some of the airports in the subgraph, with no possible shortcuts (and this would be very inefficient for both the carrier and passengers).

2.5 Two Further Applications of Subgraphs

2.5.1 Subgraphs and Node Centrality

Node centrality measures are frequently used in applied work to rank nodes by their individual "importance" in a network. Standard measures for this are designed to capture different aspects of nodal centrality, e.g., degree centrality is interpreted as the number of direct neighbours of node i; closeness centrality characterizes the (inverse of the) average shortest path from a node i to all other nodes; betweenness centrality measures the number of times that a node i acts as an "intermediary" in the sense of being on shortest paths between other pairs of nodes; and a node i is more important according to eigenvector centrality when it is directly-connected to other more important nodes; see Jackson [41, 42]. These measures have been shown to be highly correlated for many real-world and simulated networks, and thus give very similar rankings of nodes, e.g., Wuchty and Stadler [75] report high correlations between three geometric centrality measures and the logarithm of node degree, on Erdős-Rényi and scale-free random graphs; Dossin and Lawford [22] find high linear correlations between degree, closeness, betweenness and eigenvector centralities, on unweighted and weighted real-world networks defined by the domestic route service of various U.S. airlines; the main theoretical treatment is by Bloch et al. [9], who argue that standard centrality measures are all characterized by the same simple (and related) axioms. In an effort to resolve the issue of high correlation, Estrada and Rodríguez-Velázquez [27] introduce *subgraph centrality*, which measures the number of times that a node i is at the start and end of closed walks of different length, with shorter lengths having greater influence; they show that it has more discriminative power than standard centrality measures, on some real-world networks. The set of all closed walks of a given length τ can contain both cyclic and acyclic subgraphs, e.g., a length four closed walk includes the 3-star (acyclic) and the 4-circle (cyclic). Define subgraph centrality by

$$B_S(i) = \sum_{\tau=0}^{\infty} \frac{(g^\tau)_{ii}}{\tau!}. \tag{18}$$

The series (18) is bounded above by $B_S(i) \leq e^\lambda$, where λ is the principal eigenvalue of g. Estrada and Rodríguez-Velázquez [27, Theorem (4)] prove that, for a simple graph, (18) may be written as

$$B_S(i) = \sum_{j=1}^{n} (v_j)_i^2 \, e^{\lambda_j}, \tag{19}$$

where $v_1, \ldots, v_n$ are the orthonormal eigenvectors of g, with eigenvalues $\lambda_1, \ldots, \lambda_n$. We use (19) to rank the nodes in Southwest's 2013Q4 network, and compare the top-ten rankings to degree centrality, in Table 4. We also suggest a simple new measure, based on the number of non-nested subgraphs that node i belongs to. Formally, we define *subgraph membership centrality* on a graph G by

$$B_{SM}\left(\widetilde{M}_a^{(b)}; i\right) = \sum_{j \neq i} \mathbf{1}\left((i,j) \in E\left(\{\widetilde{M}_a^{(b)}\}\right)\right), \tag{20}$$

where $\{\widetilde{M}_a^{(b)}\}$ is the set of all non-nested subgraphs of type $\widetilde{M}_a^{(b)}$ in G, and $\mathbf{1}(\cdot)$ is the indicator function.

[insert Table 4 here]

Some $B_{SM}(\cdot)$ require careful interpretation: for instance, a node might have high $B_{SM}(\widetilde{M}_{11}^{(4)})$ because it is the center of many 4-stars, or frequently a spoke. To avoid this problem, we report this measure in Table 4 for regular subgraphs only: the triangle ($M_7^{(3)}$), the non-nested 4-circle ($\widetilde{M}_{30}^{(4)}$), and the 4-complete ($M_{63}^{(4)}$).[17] We find that:

- The top-ten rankings for *DC* and B_S and $B_{SM}(M_7^{(3)})$ include the same set of nodes, and are very similar. The correlations in 2013Q4 across *all* nodes, between *DC* and B_S, and between *DC* and $B_{SM}(M_7^{(3)})$, are 98.8% and 98.9% respectively. So, high degree nodes are associated with more closed walks of all lengths, and with triangles (which are closed walks of length three).

- The top-ten rankings for $B_{SM}(\widetilde{M}_{30}^{(4)})$ and $B_{SM}(M_{63}^{(4)})$ display several interesting differences to *DC*. First, Denver is the top-ranked node by 4-complete membership (still, in 2013Q4, *DC* and $B_{SM}(M_{63}^{(4)})$ are correlated at 97.5%). Second, the non-nested 4-circle $B_{SM}(\widetilde{M}_{30}^{(4)})$ rankings are very different to *DC*, and include eight "new" nodes, with Orlando top-ranked (in 2013Q4, *DC* and $B_{SM}(\widetilde{M}_{30}^{(4)})$ are correlated at only 59.5%). This shows, surprisingly given the results on B_S, that different nodes can become important when one considers membership of *particular* topologies.

- The 2013Q4 correlations between degree centrality B_{SM} for *nested* subgraphs are all very high (96% – 99%), and the latter will not give us a more informative measure here than degree centrality.

To summarize, we have proposed a simple subgraph-based centrality measure that focuses on membership of particular subgraphs, and is shown to be informative for particular topologies. For instance, we find that Dallas Love Field (DAL) and Los Angeles (LAX) are very often part of 4-circle groups of airports, but are less likely (relative to other airports) to be part of completely-connected groups. The operational reasons for this structure are still unclear. These results stand in contrast to Estrada and Rodríguez-Velázquez [27]'s centrality, which computes (weighted) membership of closed walks, including subgraphs, of *all* lengths and is, on this dataset at least, highly correlated with *DC*.[18]

2.5.2 Spatial Properties of the Triangle Subgraph

One of the distinctive characteristics of airline networks is their spatial nature: unlike many natural or social networks, the nodes (airports) have a fixed geographical location. With this in mind, we explore the dynamic spatial distribution of the triangle subgraph, chosen because "area" and "center" have a clear meaning in this case. To be precise, the area and barycenter of a triangle subgraph on a curved surface are calculated using the latitude and logitude of each node, with a great circle method. To illustrate, the triangle formed by Baltimore–Washington (BWI), Denver (DEN) and Las Vegas McCarran (LAS), with coordinates $(39.18^{\circ}, -76.67^{\circ})$, $(39.86^{\circ}, -104.67^{\circ})$, and $(36.08^{\circ}, -115.17^{\circ})$, respectively, has area 87,754 square miles, and a center located at $(38.37^{\circ}, -98.84^{\circ})$.

[insert Figure 10 here]

[17] The nodes that we have not seen before in the paper are Austin-Bergstrom (AUS), Dallas Love Field (DAL), Los Angeles (LAX), General Mitchell, Milwaukee (MKE), and San Diego (SAN).

[18] We do not suggest that B_{SM} will be more informative than B_S or *DC* in general, or for all subgraphs.

Table 4: *Comparison of top-ten node rankings in 2013Q4 by degree centrality (DC), subgraph centrality (B_S), and subgraph membership centrality (B_{SM}) for the triangle $M_7^{(3)}$, the non-nested 4-circle $\widetilde{M}_{30}^{(4)}$, and the 4-complete $M_{63}^{(4)}$. Calculated values of each centrality measure are reported in parentheses. (Section 2.5.1)*

	Centrality Measure				
Ranking	*DC*	B_S	$B_{SM}(M_7^{(3)})$	$B_{SM}(\widetilde{M}_{30}^{(4)})$	$B_{SM}(M_{63}^{(4)})$
1.	MDW (0.71)	MDW (2,681,447)	MDW (342)	MCO (446)	DEN (967)
2.	LAS (0.64)	LAS (2,510,649)	LAS (335)	TPA (353)	LAS (956)
3.	DEN (0.62)	DEN (2,449,785)	DEN (333)	DAL (295)	MDW (929)
4.	BWI (0.57)	PHX (2,116,359)	PHX (298)	LAX (194)	PHX (863)
5.	PHX (0.53)	BWI (2,017,113)	BWI (277)	AUS (190)	BWI (779)
6.	HOU (0.51)	HOU (1,729,523)	HOU (246)	MKE (181)	HOU (693)
7.	MCO (0.45)	STL (1,364,403)	STL (201)	FLL (160)	STL (591)
8.	STL (0.38)	MCO (1,296,749)	BNA (183)	SAN (152)	BNA (577)
9.	BNA (0.36)	BNA (1,240,896)	MCO (171)	MDW (150)	MCI (438)
10.	TPA (0.36)	TPA (1,128,861)	TPA (158)	MCI (136)	TPA (427)

[insert Figure 11 here]

In Figure 10, we show the general trends in the spatial distribution of triangles between 1999 and 2013. We observe that the triangle centers are evenly-distributed across the U.S. in 1999, but become progressively more concentrated in the east of the country, most notably from 2009 onwards. In Figure 11, we plot the density of the triangle subgraph area: this shows that the triangles generally become larger over time. This approach provides a straightforward graphical means of assessing the spatial evolution of clustering in a network over time: clustering (in the sense of connected triples) seems to evolve towards (at least two) nodes that are located in the eastern U.S.

3 Related Work

There is a large literature on biological motifs, that we have discussed throughout the paper. We now briefly survey other research on biological motifs, and on complex systems applied to air transportation.

3.1 Motifs

Function of individual motifs. Alon [3] comprehensively reviews experimental work on motifs in gene regulation and other biological networks, and provides evidence that different families of motifs perform precise and identifiable information-processing functions, at a cellular level, and that these networks have an inherent structural simplicity since they are based on a limited number of basic components. Mangan and Alon [50] and Hayot and Jayaprakash [35] show how motifs in natural networks may express evolved computational (Boolean) operations. Various authors have developed mathematical models for motifs, in an attempt to show how interaction patterns are related to biological function, e.g., Isihara et al. [37], although there is evidence that structural information may not be sufficient to distinguish between multiple potentially-useful functions in some cases, e.g., Ingram et al. [36].

Interrelationships and aggregation. It is clear that natural motifs are likely to interact, and another strand of research investigates how this will affect their function. Dobrin et al. [21] investigate the aggregation of motifs into clusters, in the transcriptional regulatory network of the bacterium *E. coli*. They find that most individual motifs overlap (by sharing at least one link and/or node), to create *homologous motif clusters*, and that these clusters will themselves merge into a *motif supercluster*, which has similar properties to the whole network; they suggest that this hierarchical interaction of sets of motifs, rather than isolated function, is a general property of cellular networks. Kashtan et al. [44] propose topological subgraph (motif) generalizations, created by duplicating nodes (and their edges) that have the same function, which will give larger subgraphs (motifs). Formally, a pair of nodes has the same *role* if there is an automorphism that maps one of the nodes to the other, and all nodes with the same role form a structurally equivalent class. For the undirected subgraphs that we consider (Figure 1), a node's role just corresponds to its degree *within* the subgraph. There are various ways in which nodes can be duplicated, e.g., duplicating the "center-node" role of the 3-star gives a 4-circle, while duplicating both of the "spoke" nodes of the 3-star gives a 5-star. These role-preserving generalizations will, as noted by Kashtan et al. [44], tend to have similar functionality to the original motif.

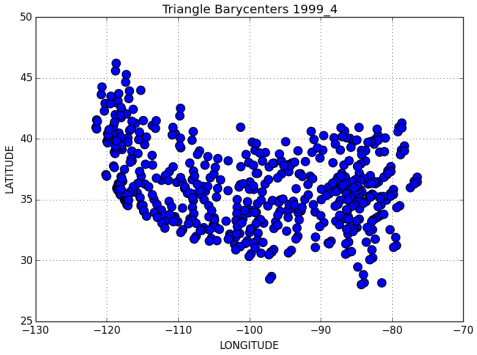

(a) *1999Q4.*

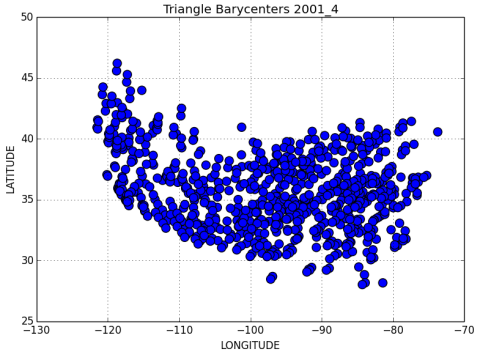

(b) *2001Q4.*

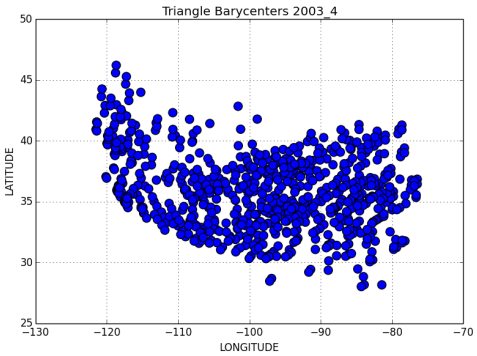

(c) *2003Q4.*

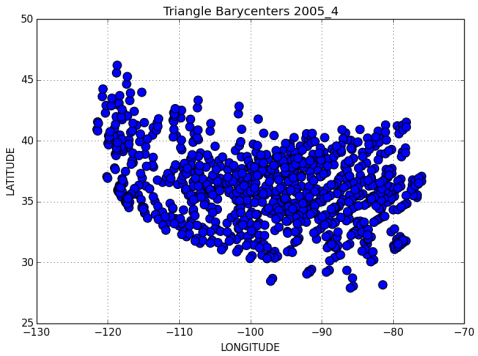

(d) *2005Q4.*

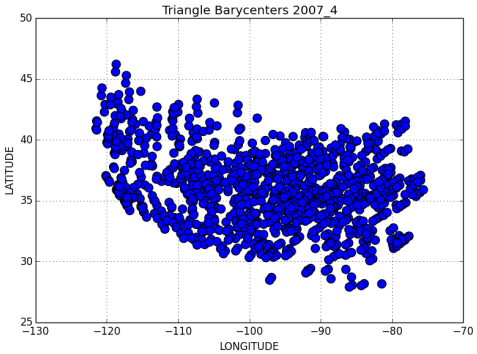

(e) *2007Q4.*

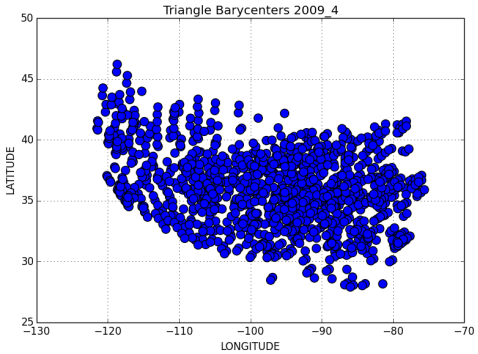

(f) *2009Q4.*

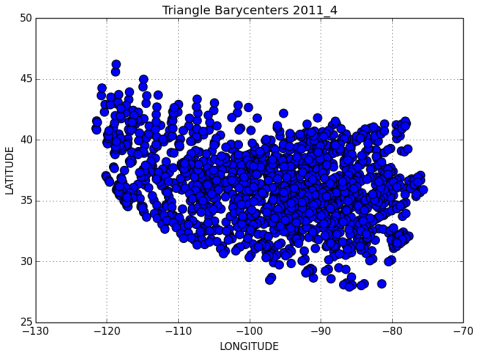

(g) *2011Q4.*

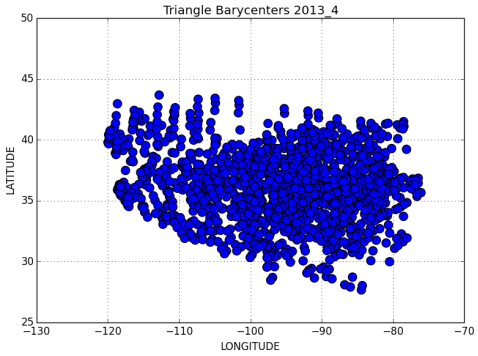

(h) *2013Q4.*

Figure 10: *Spatial distribution of the triangle subgraph center for odd-numbered years, last quarter, between 1999 and 2013 (Section 2.5.2).*

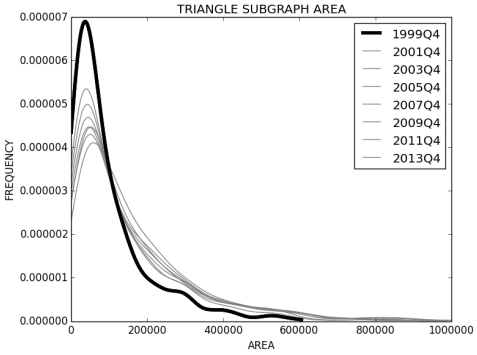

(a) *1999Q4.*

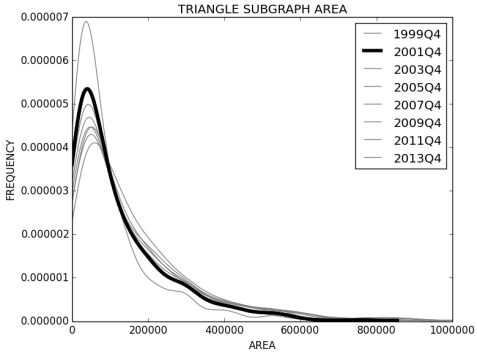

(b) *2001Q4.*

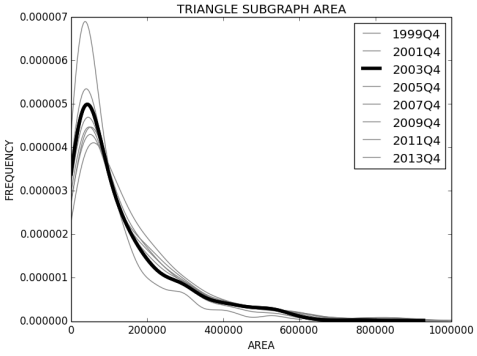

(c) *2003Q4.*

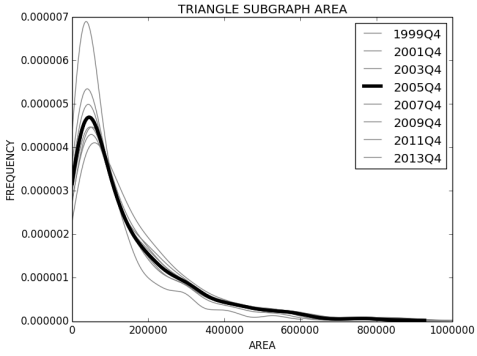

(d) *2005Q4.*

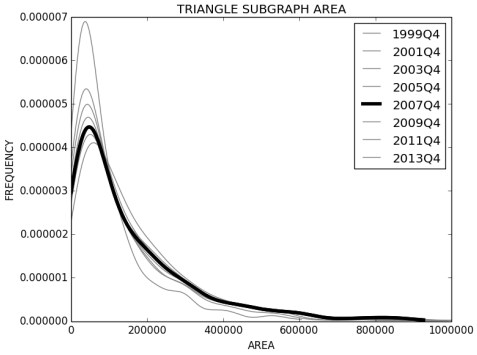

(e) *2007Q4.*

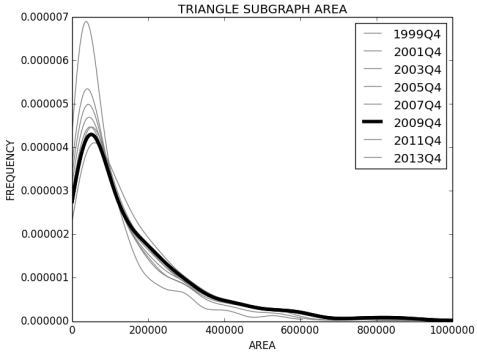

(f) *2009Q4.*

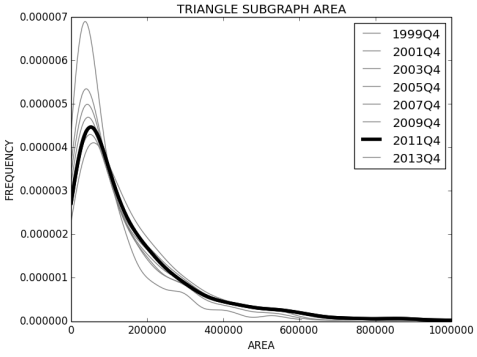

(g) *2011Q4.*

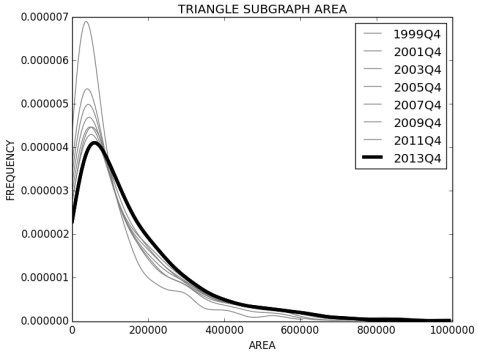

(h) *2013Q4.*

Figure 11: *Kernel density estimates of the triangle subgraph area for odd-numbered years, last quarter, between 1999 and 2013 (Section 2.5.2).*

Motifs in airline networks. Although most of the literature focuses on natural and technological networks, we have found some interesting work by Bounova [11] that, in part, applies motifs to airline route maps and (like us) investigates topology transitions in U.S. airline networks, but on monthly data over the period 1990 – 2007. She finds that most airlines have similar networks, but that Southwest is topologically distinct. Using a null randomized ensemble that matches the number of nodes and the degree sequence of the real-world network, and that we would expect to give similar results to Section 2.4.2 in our paper, for *3-node* subgraphs, she comes to a very different conclusion (Bounova [11, p.126], our emphasis added):

> Southwest brings a surprise in motif finding. *There are no significant motifs, compared to random graphs*, though we tested a few snapshots of the airline's history (1/1990, 8/1997, 8/2007) . . . Mathematically, this says that Southwest is no different from a random network.

The z-scores reported for August 2007 in Bounova [11, Figure 3-41] are all very low (roughly 0.04 – 0.16), which contradicts our findings in Figures 8 and 9. However, by augmenting the topological graph with departure frequency data used as edge-weights in a weighted graph (i.e., an edge is present only if the frequency is greater than some threshold), Bounova [11] finds some evidence that the 4-star (and a 6-node subgraph) is a motif, and remarks that "hub-spoke motifs are only a recent phenomenon in Southwest" (Bounova [11, p.127]). The 4-star motif is in essential agreement with the results presented in Figure 9 in our paper, although we find that hub-spoke motifs (i.e., 3-star and 4-star) were significant motifs from at least 1999 to 2005 and have, if anything, become *less* significant over time. We suspect that some of these differences may be due to (a) use of a different dataset and/or assumptions made during the data treatment and filtering, and (b) sensitivity to the choice of null random ensemble that was used to identify motifs.

3.2 Complex Systems Applied to Air Transportation

While there is a substantial literature on descriptive analysis of airline networks, our focus here is on research with a complex systems perspective; see Lin and Ban [48], Lordan et al. [49, Table I] and Roucolle et al. [57] for nice surveys that cover both literatures. In particular, we are interested in network resilience and generalizations of hub-spoke structure:

Core-periphery structure. Wuellner et al. [76] investigate the resilience of airline networks to a targeted removal of nodes and a random removal of edges, and find that graph connectedness and "travel times" (based on spatial geodesic lengths and intermediate airport penalties) are generally preserved. The *k-core* is defined by iterative removal of nodes (and their edges) with degree less than k, until all nodes have degree greater than or equal to k (the final network is called the k-core). Using data for 2007, the authors find that Southwest is a special case, with a large k-core structure and extreme resilience to node or edge deletion, and conclude that (Wuellner et al. [76, p.056101-1], {.} our addition):

> {Southwest} has essentially built a core network, comprising more than half of its overall destinations, which is a dense mesh of interconnected high-degree (i.e., "hub") airports.

They also report (Wuellner et al. [76, Table I]) an average path length of 1.542, that is slightly lower than the average path lengths that we plot in Figure 3c, which may be due to data treatment issues. In two related papers, Verma et al. [69, 70] analyze the core of the World Airline Network (WAN). This network is made up of more than 3,200 nodes and 18,000 edges. However, unlike the results reported above for Southwest, Verma et al. [69, 70] find that the WAN has a very small core (containing about 2.5% of all

nodes), that is almost fully connected, and is surrounded by a nearly tree-like periphery; upon removal of the core, they find that most of the WAN network is still connected.

4 Conclusions

We have explored the dynamic behaviour of small subgraphs in a relatively small transportation network defined by the route service of Southwest Airlines, which has a number of interesting features, as a growing and human-made technological system. The topology has much in common with random graphs, exhibiting "small-world" characteristics, and a possible power-law scaling between subgraph counts and the number of edges in the network that is unexpectedly robust to changes in network density. In a sense, this is curious, because the network results from careful route-level planning and strategic decision-making, based on the spatial distribution of demand and competition, as well as operational and regulatory constraints inherent in providing passenger service (e.g., availability of fleet and crew, scheduling, legal restrictions such as the Wright Amendment of 1979, etc.).[19] The network has evolved by design (from an initial state given by Southwest's network when the U.S. air transport sector was deregulated by the Airline Deregulation Act of 1978) and not at random. While short path lengths and clustering reflect the need for a carrier to provide efficient service (with few connections between airport pairs), scaling appears to be a general property of classes of graphs that satisfy a few basic conditions on, e.g., the degree distribution. We identify motifs and anti-motifs that display substantial dynamic variation, and have a rather different interpretation to those that arise in natural networks. Our results on topology evolution provide new insights into the structure of a transportation network, *that are not observable by standard measures such as node centrality and clustering*. In particular, Southwest's network has become less "starlike" over time, despite a fall in network density, but also favours unexpected local structure (e.g., circle, diamond). We illustrate how a simple new subgraph-based centrality measure can be used to identify important nodes based on membership of specific topological structures, and give graphical evidence that subgraphs can be used to explore the spatial evolution of the local structure of a network. Together, our results show that subgraph-based tools can potentially be useful in giving new qualitative and quantitative understanding of the behaviour of real-world networks, and as diagnostic tools for economic or mathematical models of network evolution.

Directions for future work. By focusing on small motifs, we are able to remain within an analytic framework for subgraph enumeration. The primary limitation of the method used is that it will not be applicable to larger motifs, of the size that are regularly considered in biology (e.g., 10 nodes and above), when the very rapid increase in the number of possible topological subgraphs necessitates the use of very fast computational methods. Some objectives for extensions of our results include (1) investigating whether our results apply to other economic or transportation networks, and finding a way to characterize the strategic behaviour of different networks based on their topology, (2) using subgraph-based methods — possibly incorporating information on edge-weights or the spatial location of nodes into the graph — and econometrics, to explain the observed strategic and dynamic decisions on market entry and exit in an economic network, (3) developing a better understanding of which classes of theoretical and real-world

[19] Similarities between Southwest's monthly network and Erdős-Rényi were also noticed by Bounova and de Weck [10, e.g. Figure 4], who describe patterns of linear correlation ("heat maps") between pairs of graph topology metrics.

graph models give rise to the scaling behaviour that we have seen here, e.g., Barrat et al. [7] report power-law decay, as a function of node degree, in the degree distribution, the total (and average) traffic handled by each airport, and in the average clustering coefficient, using data on the World Airline Network; and Song et al. [62] and Ángeles Serrano et al. [5] use renormalization to show that scale-free and small-world behaviour can arise naturally in real complex networks that are invariant/self-similar under length-scale transformations, and (4) applying state-of-the-art computational tools to search for larger motifs in such networks. We leave these interesting problems for future work.

A Proofs

Proof of Proposition 2.1. We treat each subgraph separately.

(a) $|M_3^{(3)}|$: Node i has edges to k_i neighbours, and any pair of those edges will form a star, centered on i. The result (1) follows immediately. In general, it is straightforward to count the number of b-node stars in a graph using $\sum_i \binom{k_i}{b-1}$, where a summand is set to zero if $b-1 > k_i$.

(b) $|M_7^{(3)}|$: The elements of g^3 are the number of walks of length 3 from node i to node j, and so $\mathrm{tr}\,(g^3)$ gives the total number of closed walks of length 3 in G, each of which must involve three distinct nodes i, j and x. Since there are six ways to traverse a given triangle (starting at any corner, and moving clockwise or counterclockwise), e.g., $\{(i,j),(j,x),(x,i)\}$, we divide by six in (2).

(c) $|M_{11}^{(4)}|$: The result (3) follows directly from the generalization of the argument used for $|M_3^{(3)}|$.

(d) $|M_{13}^{(4)}|$: Consider any edge $(i,j) \in E$, as the central edge in a 4-path $\{(x,i),(i,j),(j,y)\}$. Node i has $k_i - 1$ possible neighbours (for node x), and node j has $k_j - 1$ possible neighbours (for node y). There are $(k_i-1)(k_j-1)$ ways in which a neighbour of i can be paired with a neighbour of j, which gives a total of $\sum_{(i,j)\in E}(k_i-1)(k_j-1)$ across all possible central edges. This sum includes the unwanted case $x = y$, which forms the triangle with corners i, j and x. Since any of the three edges of a given triangle can be a candidate central edge (i,j) of a 4-path, we subtract $3\,|M_7^{(3)}|$ to give result (4).

(e) $|M_{15}^{(4)}|$: The tadpole subgraph can be thought of as a triangle on nodes i, j and x, with the addition of an extra edge (i,y), where $k_i > 2$. The element $\frac{1}{2}(g^3)_{ii}$ is the number of triangles attached to node i, where the division by two corrects for double-counting due to the two possible directions of travel around a given triangle. Hence, there are $\frac{1}{2}(g^3)_{ii}\,(k_i-2)$ tadpoles "centered on" node i. Result (5) follows immediately.

(f) $|M_{30}^{(4)}|$: The elements of g^4 are the number of walks of length 4 from node i to node j, and so $\mathrm{tr}\,(g^4)$ gives the total number of closed walks of length 4 in G. We proceed to prove (6) indirectly, by expressing $\mathrm{tr}\,(g^4)$ in terms of the number of circles and other walks of length 4 on a circle. Consider four distinct nodes i, j, x and y, and the circle $M_{30}^{(4)}$ with edges $\{(i,j),(j,x),(x,y),(y,i)\}$. There are *eight* ways to traverse this circle (starting at any corner, and moving clockwise or counterclockwise). However, there are two additional ways to walk from one of these nodes and back to itself in four steps, using only the four edges of the circle:

- First, there are four possible 3-stars $M_3^{(3)}$, i.e., (I) $\{(i,j),(j,x)\}$, (II) $\{(j,x),(x,y)\}$, (III) $\{(x,y),(y,i)\}$, and (IV) $\{(y,i),(i,j)\}$. Starting from node i, it is possible to build three of these: (I), (III), and (twice) (IV). Across the four nodes, each of (I)–(IV) will appear *four* times.
- Second, there are four edges in the circle. Starting from node i, it is possible to build two of these: (i,j) and (i,y). Across the four nodes, each edge in the circle will appear *twice*.

Hence, we can write $\mathrm{tr}\,(g^4) = 8|M_{30}^{(4)}| + 4|M_3^{(3)}| + 2m$, and result (6) follows directly.

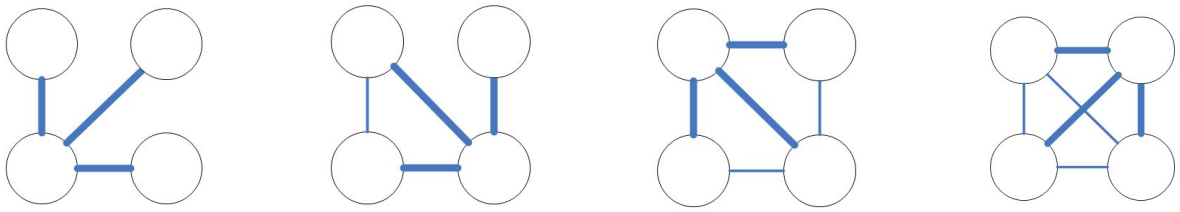

(a) *4-star* $M_{11}^{(4)}$. **(b)** *Tadpole* $M_{15}^{(4)}$. **(c)** *Diamond* $M_{31}^{(4)}$. **(d)** *4-complete* $M_{63}^{(4)}$.

Figure A.1: *Illustrative nestings of the 4-star subgraph. There is one way in which one edge can be removed from the tadpole to create a 4-star, two ways in which two edges can be removed from the diamond, and four ways in which three edges can be removed from the 4-complete.*

(g) $|M_{31}^{(4)}|$: We can think of a diamond on nodes i, j, x, and y as two distinct triangles with a common edge (i, j). Given this common edge, $(g^2)_{ij}(g)_{ij}$ represents the number of walks of length 2 between i and j, i.e., the number of distinct triangles in G that contain (i, j). A diamond is formed by any two of these triangles, and so $\binom{(g^2)_{ij}(g)_{ij}}{2}$ gives the number of distinct diamonds that can be built from a common edge (i, j). Summing across all pairs of nodes i and j will give twice the number of diamonds in G, since the edge (i, j) has two endpoints. We divide the sum by two to give result (7).

□

Proof of 4-complete subgraph count formula (8). Consider a triangle subgraph $M_7^{(3)}$ comprised of nodes j, x and y. Let each node be in the neighbourhoood $\Gamma_G(i)$ of some node i such that $i \neq j \neq x \neq y$. Hence, the four nodes i, j, x and y, and the edges between them, form a 4-complete subgraph $M_{63}^{(4)}$. The quantity $\frac{1}{6}\operatorname{tr}(g_{-i}^3)$ gives the number of 4-complete subgraphs that contain node i, where g_{-i} is the adjacency matrix induced by the neighbourhood of i. By symmetry, summing across all nodes i will give four times the total count of 4-complete subgraphs in the graph, and so we divide the sum by four to give result (8). □

Proof of Proposition 2.3. In each case, the non-nested subgraph count of H' is found by considering all subgraphs H on the same set of b nodes as H, such that $H' \subset H$, and noting the number of ways in which edges can be removed from H to obtain H'. The non-nested subgraph count $|\widetilde{M}_a^{(b)}|$ equals $|M_a^{(b)}|$ with a correction that accounts for nesting in "larger" subgraphs. For example, the 4-star $M_{11}^{(4)}$ is nested in the tadpole $M_{15}^{(4)}$, the diamond $M_{31}^{(4)}$ and the 4-complete $M_{63}^{(4)}$, as illustrated in Figure A.1. We continue to use (2) and (8) for the nested triangle and 4-complete. We treat each subgraph separately but, for convenience of exposition, not in order.

[insert Figure A.1 here]

(a) $|\widetilde{M}_3^{(3)}|$: To create a 3-star, there are three ways to remove one edge from the triangle. Result (10) follows immediately.

(b) $|\widetilde{M}_{31}^{(4)}|$: To create a diamond, there are six ways to remove one edge from the 4-complete. Result (15) follows immediately.

(c) $|\widetilde{M}_{30}^{(4)}|$: To create a 4-circle, there is one way to remove one edge from the diamond, and three ways to remove two edges (with no common nodes) from the 4-complete. Hence,

$$|\widetilde{M}_{30}^{(4)}| = |M_{30}^{(4)}| - |\widetilde{M}_{31}^{(4)}| - 3\,|M_{63}^{(4)}|,$$

and (14) follows from (15).

(d) $|\widetilde{M}_{15}^{(4)}|$: To create a tadpole, there are four ways to remove one edge from the diamond, and twelve ways to remove two edges (with a common node) from the 4-complete. Hence,

$$|\widetilde{M}_{15}^{(4)}| = |M_{15}^{(4)}| - 4\,|\widetilde{M}_{31}^{(4)}| - 12\,|M_{63}^{(4)}|,$$

and (13) follows from (15).

(e) $|\widetilde{M}_{13}^{(4)}|$: To create a 4-path, there are two ways to remove one edge from a tadpole, four ways to remove one edge from a 4-circle, six ways to remove two edges from a diamond, and twelve ways to remove three edges from a 4-complete. So,

$$|\widetilde{M}_{13}^{(4)}| = |M_{13}^{(4)}| - 2\,|\widetilde{M}_{15}^{(4)}| - 4\,|\widetilde{M}_{30}^{(4)}| - 6\,|\widetilde{M}_{31}^{(4)}| - 12\,|M_{63}^{(4)}|,$$

and (12) follows from (13), (14) and (15).

(f) $|\widetilde{M}_{11}^{(4)}|$: As illustrated in Figure A.1, to create a 4-star, there is one way to remove one edge from a tadpole, two ways to remove two edges from a diamond, and four ways to remove three edges (a triangle) from the 4-complete. Then,

$$|\widetilde{M}_{11}^{(4)}| = |M_{11}^{(4)}| - |\widetilde{M}_{15}^{(4)}| - 2\,|\widetilde{M}_{31}^{(4)}| - 4\,|M_{63}^{(4)}|,$$

and (11) follows from (13) and (15).

□

Proof of Proposition 2.4. For each of the statements in the Proposition, we could present a formal proof. For example, consider the expected number of triangles (see Proposition 2.4). For every subgraph $S \subset G(n,p)$, let Z_S be the event "S is a triangle", and let X_S be its indicator random variable. Then, $\mathrm{E}(X_S) = \Pr(Z_S) = p^3$, where $\Pr(\cdot)$ is the probability of an event. Define $Y = \sum_{|V(S)|=3} X_S$. By linearity of expectation, $\mathrm{E}(Y) = \sum_{|V(S)|=3} \mathrm{E}(X_S)$, and the result follows. Alternatively, we could directly specialize the formulae in Proposition 2.1 to K_n. For example, the number of triangles is generally given by $\frac{1}{6}\,\mathrm{tr}\,(g^3)$, and it is easy to see that $(g^3)_{ii} = (n-1)(n-2)$ for K_n, so that $\frac{1}{6}\,\mathrm{tr}\,(g^3) = \binom{n}{3}$. However, we instead present more informal proofs of each statement, based directly on the properties of K_n, that we feel are more intuitive and accessible. Using linearity of expectation as above, it is sufficient to find the number of each subgraph S of interest in K_n, and then to multiply this count by $p^{|E(S)|}$ to give the count in $G(n,p)$.

(a) $|M_3^{(3)}|$: Each node in K_n can be the center of the 3-star, giving $n\binom{n-1}{2} = 3\binom{n}{3}$ 3-stars in K_n.

(b) $|M_7^{(3)}|$: There are $\binom{n}{3}$ triangles in K_n.

(c) $|M_{11}^{(4)}|$: Each of the n nodes in K_n can be the center of the 4-star, and so there are a total of $n\binom{n-1}{3} = 4\binom{n}{4}$ 4-stars in K_n. This is a direct generalization of the proof of $|M_3^{(3)}|$.

(d) $|M_{13}^{(4)}|$: We can choose 4 nodes in $\binom{n}{4}$ ways, and they can be linked by a maximum of 6 edges. There are $\binom{6}{3} = 20$ combinations of 3 edges on these 4 nodes, including 4 that will give a triangle (and an isolated node) and 4 that will give a 4-star. Hence, there are 12 possible 4-paths on 4 nodes.

(e) $|M_{15}^{(4)}|$: There are $\binom{n}{3}$ triangles in K_n. Any of the 3 corners of each triangle can be the "center" (degree 3 node) of a tadpole, and links to $(n-3)$ other nodes, forming a tadpole in each case.

(f) $|M_{30}^{(4)}|$: The argument is similar to that used for $|M_{13}^{(4)}|$. We can choose 4 nodes in $\binom{n}{4}$ ways, and they can be linked by a maximum of 6 edges. There are $\binom{6}{4} = 15$ combinations of 4 edges on these 4 nodes, including 12 that will give a tadpole (there are 4 triangles, and 3 ways to add an additional edge for each). Hence, there are 3 possible circles on 4 nodes. We can also show this directly by labelling the nodes of a circle i, j, x and y: corner i can have opposite (non-adjacent) corner j, x or y.

(g) $|M_{31}^{(4)}|$: We can choose 4 nodes in $\binom{n}{4}$ ways, and there are 6 ways to link them with 5 edges, each of which will generate a diamond with a different common edge (between the two triangles).

(h) $|M_{63}^{(4)}|$: We can choose 4 nodes in $\binom{n}{4}$ ways, and there is only one way to link them with 6 edges.

□

B Additional Figures

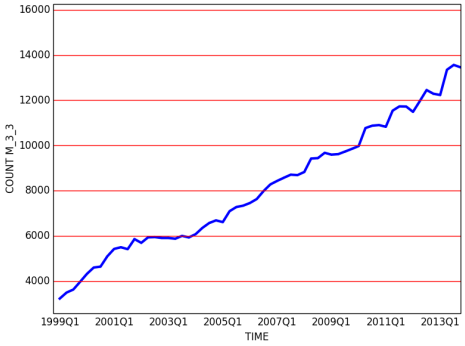

(a) *3-star* $M_3^{(3)}$.

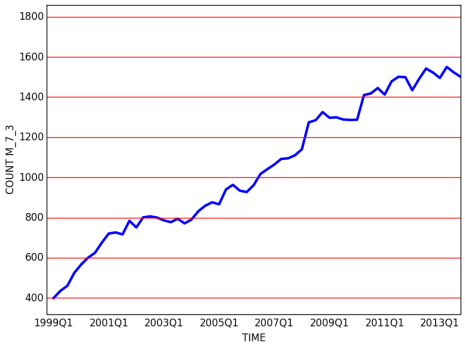

(b) *Triangle* $M_7^{(3)}$.

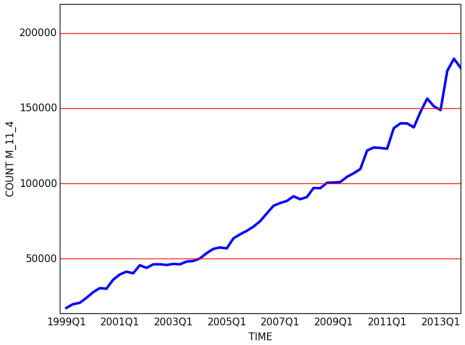

(c) *4-star* $M_{11}^{(4)}$.

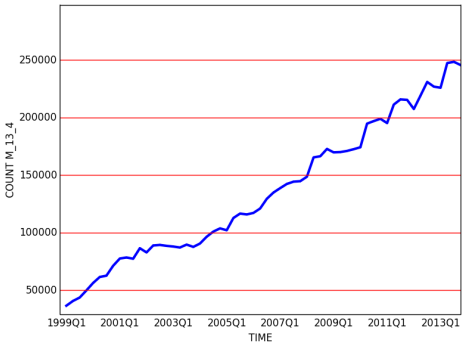

(d) *4-path* $M_{13}^{(4)}$.

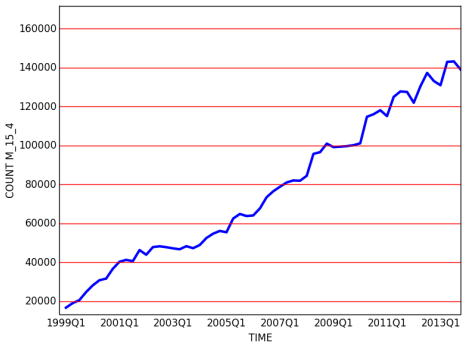

(e) *Tadpole* $M_{15}^{(4)}$.

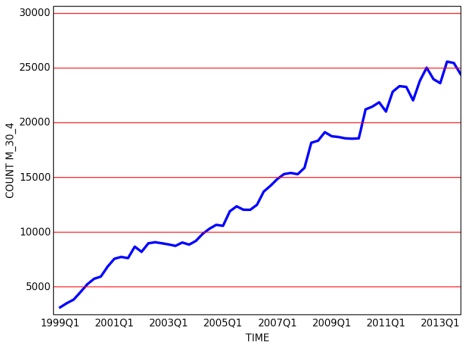

(f) *4-circle* $M_{30}^{(4)}$.

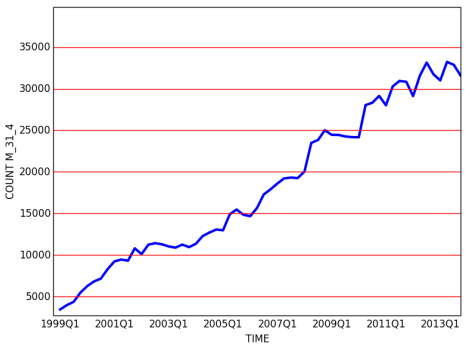

(g) *Diamond* $M_{31}^{(4)}$.

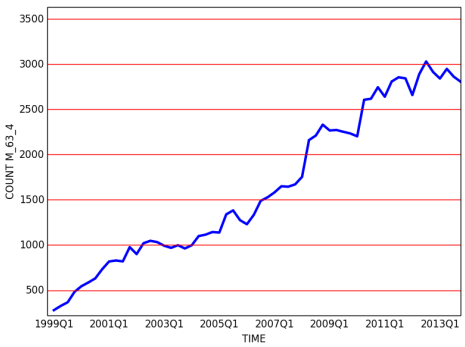

(h) *4-complete* $M_{63}^{(4)}$.

Figure B.1: *Nested subgraph counts by analytic formulae (Section 2.2).*

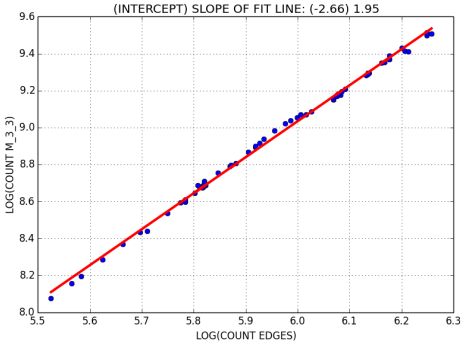

(a) *3-star* $M_3^{(3)}$.

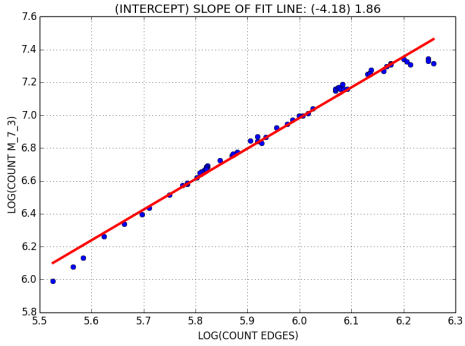

(b) *Triangle* $M_7^{(3)}$.

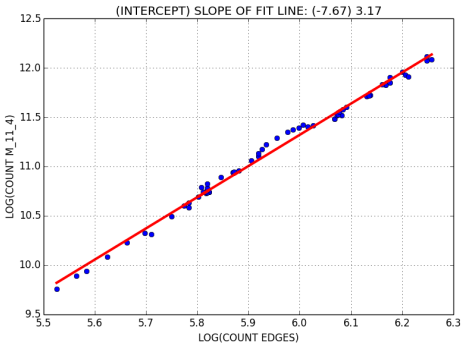

(c) *4-star* $M_{11}^{(4)}$.

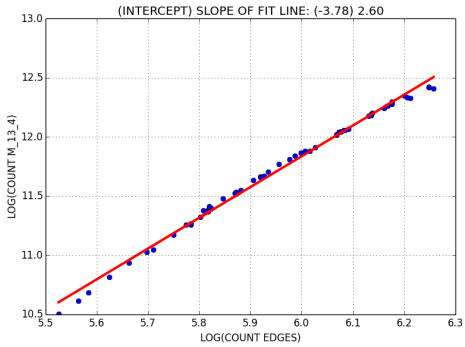

(d) *4-path* $M_{13}^{(4)}$.

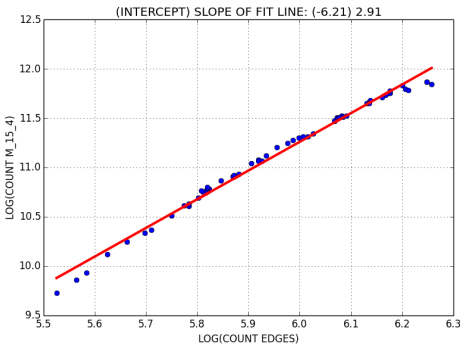

(e) *Tadpole* $M_{15}^{(4)}$.

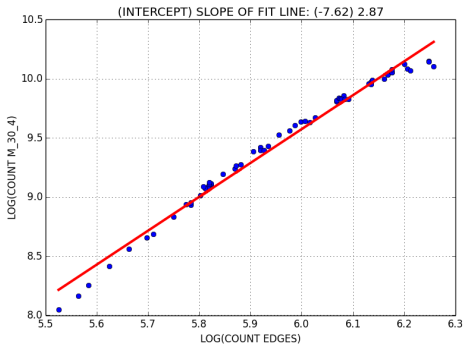

(f) *4-circle* $M_{30}^{(4)}$.

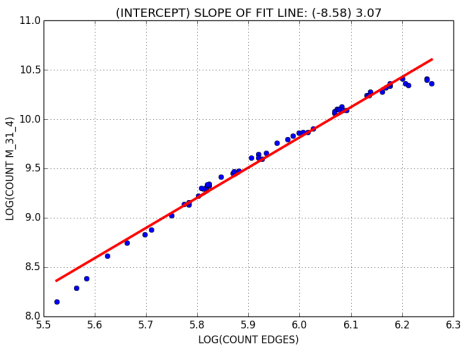

(g) *Diamond* $M_{31}^{(4)}$.

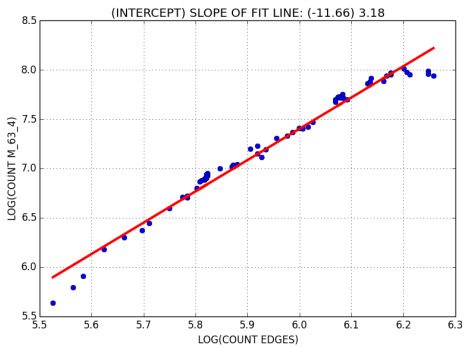

(h) *4-complete* $M_{63}^{(4)}$.

Figure B.2: *Log–log plots of number of edges m against nested subgraph count* $|M_a^{(b)}|$ *(Section 2.3).*

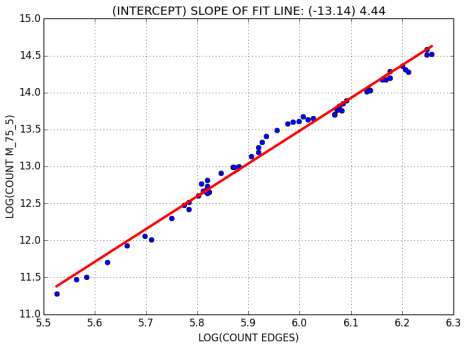

(a) *5-star* $M_{75}^{(5)}$.

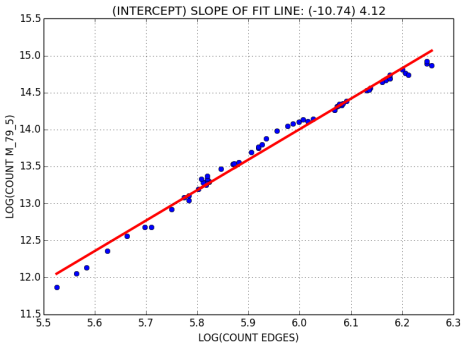

(b) *Cricket* $M_{79}^{(5)}$.

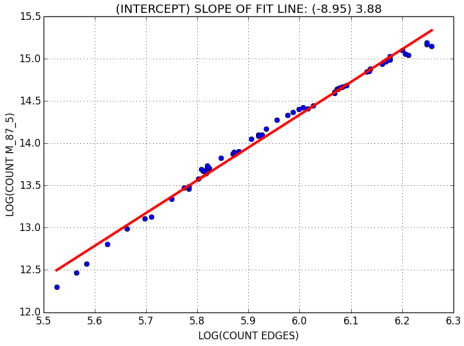

(c) *Bull* $M_{87}^{(5)}$.

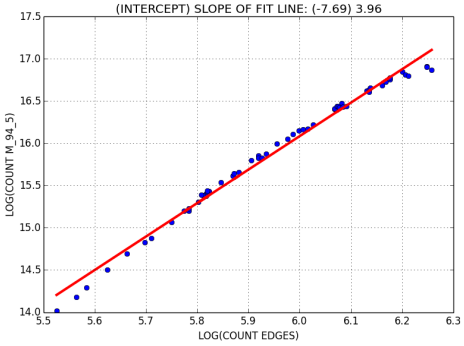

(d) *Banner* $M_{94}^{(5)}$.

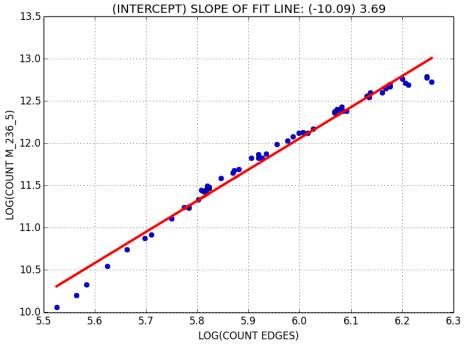

(e) *5-circle* $M_{236}^{(5)}$.

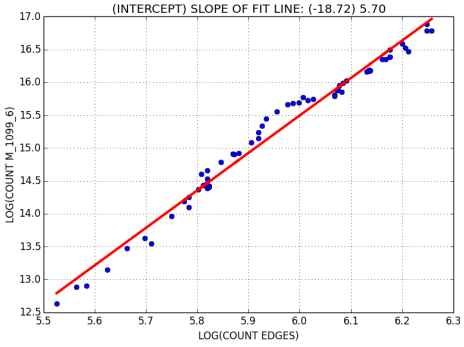

(f) *6-star* $M_{1099}^{(6)}$.

Figure B.3: *Log–log plots of number of edges m against nested subgraph count* $|M_a^{(b)}|$ *(Section 2.3.2).*

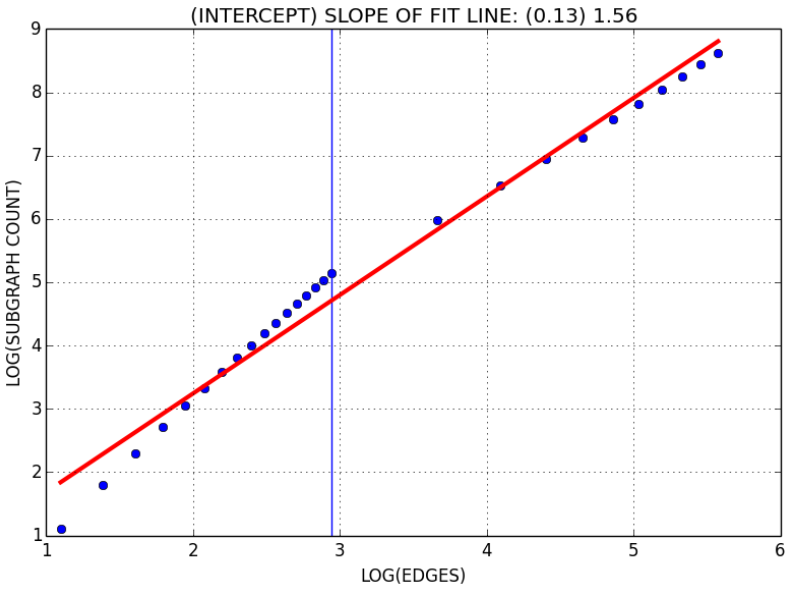

Figure B.4: *Averaging of scaling factor by regression fit, for toy regime-switching model (Section 2.3.3), illustrated using simulated data, with $l = 4, \ldots, n = 30$, and breakpoint $n^\star = 20$ between Regimes 1 and 2.*

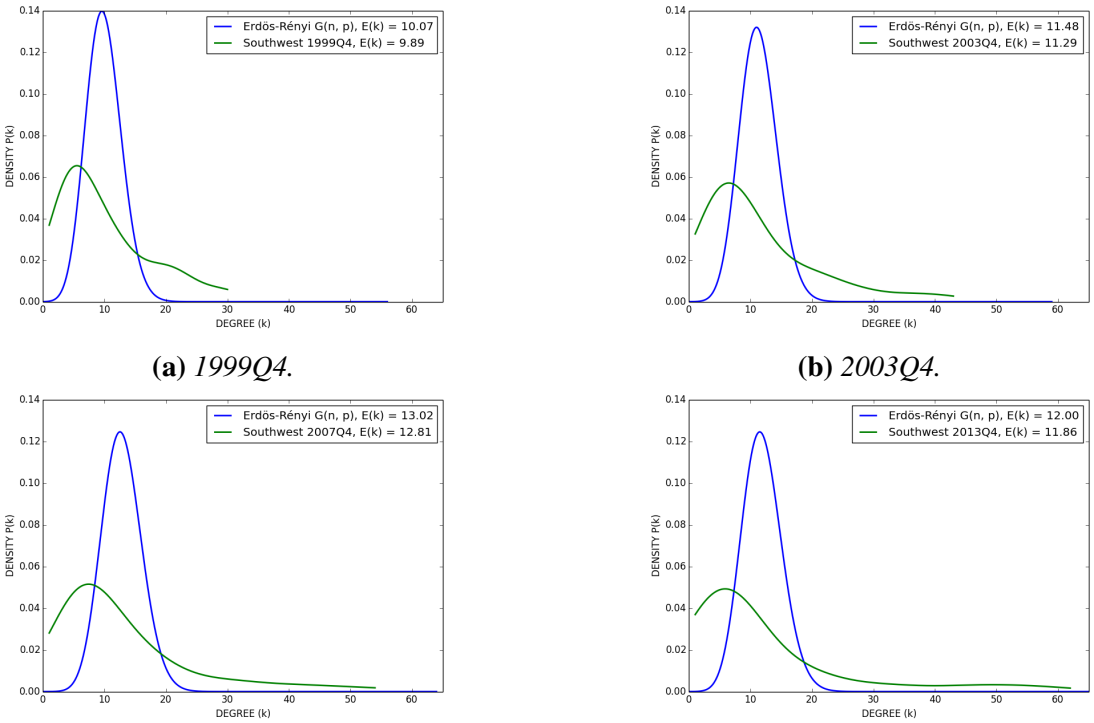

(a) *1999Q4.* **(b)** *2003Q4.*

(c) *2007Q4.* **(d)** *2013Q4.*

Figure B.5: *Gaussian kernel density estimates corresponding to the degree distribution $P(k)$ of Southwest's network, not correcting for edge-effects; and the binomial degree distribution of the Erdős-Rényi graph $G(n, p)$ with edge-formation probability $p = d(G)$ (Section 2.4.2). Note that the Gaussian kernel does not correct for potential edge-effects at $k = 0$.*

C Subgraph Notation

We denote b-node subgraphs by $M_a^{(b)}$, where a is a decimal number defined as follows (see Example C.1):

1. Choose an arbitrary labelling of the nodes of the subgraph (from 1 to b), to give a subgraph G'.
2. Find all subgraphs that are isomorphic to G', and list their adjacency matrices.
3. Use the upper-triangular elements of each adjacency matrix, including leading zeros, to give binary representations, e.g., 111000_2 and 100110_2 and 010101_2 and 001011_2, respectively.
4. Find the decimal representation of each binary number, and set b equal to the minimum of these, e.g., in the example, we have 56_{10} and 38_{10} and 21_{10} and 11_{10}; so, we use $M_{11}^{(4)}$ to denote the 4-star.

Example C.1 (Notation)**.**

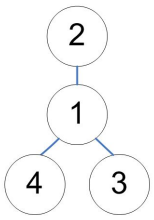

$$= \begin{array}{c} \\ 1 \\ 2 \\ 3 \\ 4 \end{array} \begin{array}{c} \begin{array}{cccc} 1 & 2 & 3 & 4 \end{array} \\ \begin{pmatrix} 0 & 1 & 1 & 1 \\ 1 & 0 & 0 & 0 \\ 1 & 0 & 0 & 0 \\ 1 & 0 & 0 & 0 \end{pmatrix} \end{array} \cong \begin{array}{c} \\ 1 \\ 2 \\ 3 \\ 4 \end{array} \begin{array}{c} \begin{array}{cccc} 1 & 2 & 3 & 4 \end{array} \\ \begin{pmatrix} 0 & 1 & 0 & 0 \\ 1 & 0 & 1 & 1 \\ 0 & 1 & 0 & 0 \\ 0 & 1 & 0 & 0 \end{pmatrix} \end{array} \cong \begin{array}{c} \\ 1 \\ 2 \\ 3 \\ 4 \end{array} \begin{array}{c} \begin{array}{cccc} 1 & 2 & 3 & 4 \end{array} \\ \begin{pmatrix} 0 & 0 & 1 & 0 \\ 0 & 0 & 1 & 0 \\ 1 & 1 & 0 & 1 \\ 0 & 0 & 1 & 0 \end{pmatrix} \end{array} \cong \begin{array}{c} \\ 1 \\ 2 \\ 3 \\ 4 \end{array} \begin{array}{c} \begin{array}{cccc} 1 & 2 & 3 & 4 \end{array} \\ \begin{pmatrix} 0 & 0 & 0 & 1 \\ 0 & 0 & 0 & 1 \\ 0 & 0 & 0 & 1 \\ 1 & 1 & 1 & 0 \end{pmatrix} \end{array}.$$

References

[1] V. Aguirregabiria and C.-Y. Ho. A dynamic oligopoly game of the US airline industry: Estimation and policy experiments. *Journal of Econometrics*, 168:156–173, 2012.

[2] N. Alon, R. Yuster, and U. Zwick. Finding and counting given length cycles. *Algorithmica*, 17: 209–223, 1997.

[3] U. Alon. Network motifs: Theory and experimental approaches. *Nature Reviews Genetics*, 8: 450–461, 2007.

[4] O. Angel, R. van der Hofstad, and C. Holmgren. Limit laws for self-loops and multiple edges in the configuration model. Technical Report arXiv:1603.07172v2, 2017. (available at: `http://arxiv.org/abs/1603.07172`).

[5] M. Ángeles Serrano, D. Krioukov, and M. Boguñá. Self-similarity of complex networks and hidden metric spaces. *Physical Review Letters*, 100:078701, 2008.

[6] A.-L. Barabási. *Network Science*. Cambridge University Press, 2016.

[7] A. Barrat, M. Barthélemy, R. Pastor-Satorras, and A. Vespignani. The architecture of complex weighted networks. *PNAS*, 101:3747–3752, 2004.

[8] A. Björklund, R. Pagh, V. Vassilevska Williams, and U. Zwick. Listing triangles. In *ICALP 14 (International Colloquium on Automata, Languages, and Programming)*, 2014.

[9] F. Bloch, M.O. Jackson, and P. Tebaldi. Centrality measures in networks. Technical Report arXiv:1608.05845v1, 2016. (available at: `http://arxiv.org/pdf/1608.05845v1.pdf`).

[10] G. Bounova and O. de Weck. Overview of metrics and their correlation patterns for multiple-metric topology analysis on heterogeneous graph ensembles. *Physical Review E*, 85:016117, 2012.

[11] G.A. Bounova. *Topological evolution of networks: Case studies in the US airlines and language Wikipedias*. PhD thesis, Massachusetts Institute of Technology, 2009.

[12] C. Bron and J. Kerbosch. Algorithm 457: Finding all cliques of an undirected graph. *Communications of the ACM*, 16:575–577, 1973.

[13] L. Chen, X. Qu, M. Cao, Y. Zhou, W. Li, B. Liang, W. Li, W. He, C. Feng, X. Jia, and Y. He. Identification of breast cancer patients based on human signaling network motifs. *Scientific Reports*, 3:3368, 2013.

[14] S. Chu and J. Cheng. Triangle listing in massive networks. *ACM Transactions on Knowledge Discovery from Data*, 6:17:1–17:32, 2012.

[15] F. Ciliberto and E. Tamer. Market structure and multiple equilibria in airline markets. *Econometrica*, 77:1791–1828, 2009.

[16] A. Clauset, C.R. Shalizi, and M.E.J. Newman. Power-law distributions in empirical data. *SIAM Review*, 51:661–703, 2009.

[17] D. Coppersmith and S. Winograd. Matrix multiplication via arithmetic progressions. *Journal of Symbolic Computation*, 9:251–280, 1990.

[18] T.H. Cormen, C.E. Leiserson, R.L. Rivest, and C. Stein. *Introduction to Algorithms*. MIT Press, 3rd edition, 2009.

[19] M. Dai, Q. Liu, and K. Serfes. Is the effect of competition on price dispersion non-monotonic? Evidence from the U.S. airline industry. *Review of Economics and Statistics*, 96:161–170, 2014.

[20] R. Diestel. *Graph Theory*. Springer, 5th edition, 2017.

[21] R. Dobrin, Q.K. Beg, A.-L. Barabási, and Z.N. Oltvai. Aggregation of topological motifs in the *Escherichia coli* transcriptional regulatory network. *BMC Bioinformatics*, 5:10, 2004.

[22] A. Dossin and S. Lawford. Weighted network centrality measures: with application to U.S. domestic airlines. DEVI / ENAC unpublished report, 2017.

[23] S.N. Durlauf. Complexity and empirical economics. *Economic Journal*, 115:F225–F243, 2005.

[24] R.W. Eglese. Simulated annealing: A tool for operational research. *European Journal of Operational Research*, 46:271–281, 1990.

[25] E. Estrada. *The Structure of Complex Networks*. Oxford University Press, 2011.

[26] E. Estrada and P.A. Knight. *A First Course in Network Theory*. Oxford University Press, 2015.

[27] E. Estrada and J.A. Rodríguez-Velázquez. Subgraph centrality in complex networks. *Physical Review E*, 71:056103, 2005.

[28] Facebook. Press Release: Facebook Reports Second Quarter 2017 Results. `http://investor.fb.com/investor-news/default.aspx` July 26 2017. `http://s21.q4cdn.com/399680738/files/doc_news/2017/FB-Q2'17-Earnings-Release.pdf` (Retrieved on September 6, 2017).

[29] D.C. Fisher and J. Ryan. Bounds on the number of complete subgraphs. *Discrete Mathematics*, 103: 313–320, 1992.

[30] X. Gabaix. Power laws in economics and finance. *Annual Review of Economics*, 1:255–293, 2009.

[31] X. Gabaix. Power laws in economics: An introduction. *Journal of Economic Perspectives*, 30: 185–206, 2016.

[32] X. Gabaix, P. Gopikrishnan, V. Plerou, and H.E. Stanley. A theory of power-law distributions in financial market fluctuations. *Nature*, 423:267–270, 2003.

[33] A. Goolsbee and C. Syverson. How do incumbents respond to the threat of entry? Evidence from the major airlines. *Quarterly Journal of Economics*, 123:1611–1633, 2008.

[34] F. Harary and A.J. Schwenk. The spectral approach to determining the number of walks in a graph. *Pacific Journal of Mathematics*, 80:443–449, 1979.

[35] F. Hayot and C. Jayaprakash. A feedforward loop motif in transcriptional regulation: Induction and repression. *Journal of Theoretical Biology*, 234:133–143, 2005.

[36] P.J. Ingram, M.P.H. Stumpf, and J. Stark. Network motifs: Structure does not determine function. *BMC Genomics*, 7:108, 2006.

[37] S. Isihara, K. Fujimoto, and T. Shibata. Cross talking of network motifs in gene regulation that generates temporal pulses and spatial stripes. *Genes to Cells*, 10:1025–1038, 2005.

[38] R. Itzhack, Y. Mogilevski, and Y. Louzoun. An optimal algorithm for counting network motifs. *Physica A*, 381:482–490, 2007.

[39] S. Itzkovitz and U. Alon. Subgraphs and network motifs in geometric networks. *Physical Review E*, 71:026117, 2005.

[40] S. Itzkovitz, R. Levitt, N. Kashtan, R. Milo, M. Itzkovitz, and U. Alon. Coarse-graining and self-dissimilarity of complex networks. *Physical Review E*, 71:016127, 2005.

[41] M.O. Jackson. *Social and Economic Networks*. Princeton University Press, 2008.

[42] M.O. Jackson. An overview of social networks and economic applications. In J. Benhabib, A. Bisin, and M.O. Jackson, editors, *Handbook of Social Economics*. North Holland, 2011.

[43] D. Jungnickel. *Graphs, Networks and Algorithms*. Springer, 3rd edition, 2008.

[44] N. Kashtan, S. Itzkovitz, R. Milo, and U. Alon. Topological generalizations of network motifs. *Physical Review E*, 70:031909, 2004.

[45] N. Kashtan, S. Itzkovitz, R. Milo, and U. Alon. Efficient sampling algorithm for estimating subgraph concentrations and detecting network motifs. *Bioinformatics*, 20:1746–1758, 2004.

[46] S. Khakabimamaghani, I. Sharafuddin, N. Dichter, I. Koch, and A. Masoudi-Nejad. QuateXelero: An accelerated exact network motif detection algorithm. *PloS ONE*, 8:e68073, 2013.

[47] J. Leskovec and A. Krevl. SNAP Datasets: Stanford Large Network Dataset Collection. `http://snap.stanford.edu/data` 2017.

[48] J. Lin and Y. Ban. The evolving network structure of US airline system during 1990-2010. *Physica A*, 410:302–312, 2014.

[49] O. Lordan, J.M. Sallan, and P. Simo. Study of the topology and robustness of airline route networks from the complex network approach: a survey and research agenda. *Journal of Transport Geography*, 37:112–120, 2014.

[50] S. Mangan and U. Alon. Structure and function of the feed-forward loop network motif. *PNAS*, 100: 11980–11985, 2003.

[51] R. Milo, S. Shen-Orr, S. Itzkovitz, N. Kashtan, D. Chklovskii, and U. Alon. Network motifs: Simple building blocks of complex networks. *Science*, 298:824–827, 2002.

[52] A. Mrvar and V. Batagelj. Analysis and visualization of large networks with program package Pajek. *Complex Adaptive Systems Modeling*, 4:6, 2016.

[53] M.E.J. Newman. The structure and function of complex networks. *SIAM Review*, 45:167–256, 2003.

[54] M.E.J. Newman. Random graphs with clustering. *Physical Review Letters*, 103:058701, 2009.

[55] E. Orduña-Malea, J.M. Ayllón, A. Martín-Martín, and E.D. López-Cózar. Methods for estimating the size of Google Scholar. Technical Report arXiv:1506.03009v1, 2015. (available at: `http://arxiv.org/abs/1506.03009`).

[56] R.J. Prill, P.A. Iglesias, and A. Levchenko. Dynamic properties of network motifs contribute to biological network organization. *PLoS Biology*, 3:1881–1892, 2005.

[57] C. Roucolle, T. Seregina, and M. Urdanoz. Measuring airline networks: Comprehensive indicators. ENAC unpublished report, 2017.

[58] A. Ruciński. When are small subgraphs of a random graph normally distributed? *Probability Theory and Related Fields*, 78:1–10, 1988.

[59] W.E. Schlauch and K.A. Zweig. Influence of the null-model on motif detection. In *ASONAM 15 (Advances in Social Networks Analysis and Mining)*, 2015.

[60] F. Schreiber and H. Schwöbbermeyer. Frequency concepts and pattern detection for the analysis of motifs in networks. In *Transactions on Computational Systems Biology III*, pages 89–104, 2005.

[61] S.S. Shen-Orr, R. Milo, S. Mangan, and U. Alon. Network motifs in the transcriptional regulation network of *Escherichia coli*. *Nature Genetics*, 31:64–68, 2002.

[62] C. Song, S. Havlin, and H.A. Makse. Self-similarity of complex networks. *Nature*, 433:392–395, 2005.

[63] O. Sporns and R. Kötter. Motifs in brain networks. *PLoS Biology*, 2:1910–1918, 2004.

[64] N.T.L. Tran, S. Mohan, Z. Xu, and C.-H. Huang. Current innovations and future challenges of network motif detection. *Briefings in Bioinformatics*, 16:497–525, 2014.

[65] Twitter. Press Release: Twitter Announces Second Quarter 2017 Results. `http://investor.twitterinc.com/results.cfm` July 27 2017. `http://files.shareholder.com/downloads/AMDA-2F526X/5135079665x0x951003/11DEB964-E7A5-43F8-96E2-D074A947255B/TWTR_Q2_17_Earnings_Press_Release.pdf` (Retrieved on September 6, 2017).

[66] V. Vassilevska. Efficient algorithms for clique problems. *Information Processing Letters*, 109: 254–257, 2009.

[67] V. Vassilevska Williams. Multiplying matrices in $O(n^{2.373})$ time. Mimeo, Available at: `\http://people.csail.mit.edu/virgi/matrixmult-f.pdf` 2014.

[68] V. Vassilevska Williams, J.R. Wang, R. Williams, and H. Yu. Finding four-node subgraphs in triangle time. In *SODA 15 (ACM-SIAM Symposium on Discrete Algorithms)*, 2015.

[69] T. Verma, N.A.M. Araújo, and H.J. Herrmann. Revealing the structure of the world airline network. *Scientific Reports*, 4:5638, 2014.

[70] T. Verma, F. Russmann, N.A.M. Araújo, J. Nagler, and H.J. Herrmann. Emergence of core-peripheries in networks. *Nature Communications*, 7:10441, 2016.

[71] D.J. Watts. Networks, dynamics, and the small-world phenomenon. *American Journal of Sociology*, 105:493–527, 1999.

[72] D.J. Watts and S.H. Strogatz. Collective dynamics of 'small-world' networks. *Nature*, 393:440–442, 1998.

[73] E. Wong, B. Baur, S. Quader, and C.-H. Huang. Biological network motif detection: Principles and practice. *Briefings in Bioinformatics*, 13:202–215, 2011.

[74] S.F. Wu, W.Y. Qian, J.W. Zhang, Y.B. Yang, Y. Liu, Y. Dong, Z.B. Zhang, Y.P. Zhu, and Y.J. Feng. Network motifs in the transcriptional regulation network of cervical carcinoma cells respond to EGF. *Archives of Gynecology and Obstetrics*, 287:771–777, 2013.

[75] S. Wuchty and P.F. Stadler. Centers of complex networks. *Journal of Theoretical Biology*, 223: 45–53, 2003.

[76] D.R. Wuellner, S. Roy, and R.M. D'Souza. Resilience and rewiring of the passenger airline networks in the United States. *Physical Review E*, 82:056101, 2010.

[77] E. Yeger-Lotem, S. Sattath, N. Kashtan, S. Itzkovitz, R. Milo, R.Y. Pinter, and U. Alon. Network motifs in integrated cellular networks of transcription–regulation and protein–protein interaction. *PNAS*, 101:5934–5939, 2004.